JCTC Journal of Chemical Theory and Computation

Article

pubs.acs.org/JCTC

A Density Functional with Spherical Atom Dispersion Terms

Amy Austin,[†] George A. Petersson,*[,†] Michael J. Frisch,[†,‡] Frank J. Dobek,[†] Giovanni Scalmani,[‡] and Kyle Throssell[†]

[†]Hall-Atwater Laboratories of Chemistry, Wesleyan University, Middletown, Connecticut 06459, United States

[‡]Gaussian, Inc., 340 Quinnipiac Street Building 40, Wallingford, Connecticut 06492, United States

Supporting Information

ABSTRACT: A new hybrid density functional, APF, is introduced, which avoids the spurious long-range attractive or repulsive interactions that are found in most density functional theory (DFT) models. It therefore provides a sound baseline for the addition of an empirical dispersion correction term, which is developed from a spherical atom model (SAM). The APF-D empirical dispersion model contains nine adjustable parameters that were selected based on a very small training set (15 noble gas dimers and 4 small hydrocarbon dimers), along with two computed atomic properties (ionization potential and effective atomic polarizability) for each element. APF-D accurately describes a large portion of the potential energy surfaces of complexes of noble gas atoms with various diatomic molecules involving a wide range of elements and of dimers of small hydrocarbons, and it reproduces the relative conformational energies of organic molecules. The accuracy for these weak interactions is comparable to that of CCSD(T)/aug-cc-pVTZ calculations. The accuracy in predicting the geometry of hydrogen bond complexes is competitive with other models involving DFT and empirical dispersion.

1. INTRODUCTION

The concept of Model Chemistry[1] introduced by John Pople has transformed computational quantum chemistry into a practical tool that is routinely employed by the nonspecialist.[2] The models that enjoy widest applicability typically rely on Density Functional Theory (DFT) to determine geometries and zero point vibrational energies.[3,4] However, the nonlocal nature of dispersion forces requires a functional involving either a six dimensional integral[5−14] or an empirical add-on[15−26] to achieve a proper R^{-6} long-range behavior.[14,27,28] The omission of these forces makes popular functionals such as B3LYP[29] unsuitable for systems in which weak interactions play a major role. In this paper, we introduce a new combination of a density functional and an empirical dispersion add-on. The density functional is chosen to eliminate spurious interactions as much as possible prior to the inclusion of the empirical add-on correction, which then is designed to reproduce the physics of dispersion between spherical atoms.

The London dispersion interaction energy between two nonbonded atoms is usually expressed as a multipole expansion:[30,31]

$$V(R_{AB}) = \frac{C_{6,AB}}{R_{AB}^6} + \frac{C_{8,AB}}{R_{AB}^8} + \frac{C_{10,AB}}{R_{AB}^{10}} + \cdots \quad (1)$$

Our empirical dispersion add-on starts from the definition of a novel atom−atom pairwise potential function to describe dispersion forces. Such potential arises from the interaction of two spherical shells of polarizable medium, and it has accuracy comparable to the leading three terms of the point multipole expansion in eq 1. This Spherical Atom Model (SAM) can, in principle, be combined with *ab initio* methods such as Hartree−Fock (HF) and DFT as well as semiempirical methods, or Molecular Mechanics (MM) force fields. In this paper, we focus on the development of a DFT-SAM model for the accurate prediction of both energies and molecular structure. Moreover, we aim to maintain consistent accuracy within a region of the Potential Energy Surface (PES) extending from the minimum all the way to the asymptotic dissociation limit, thereby providing a good description of both the curvature of the PES close to the minimum and the R^{-6} decay of the interaction energy. A consistent accuracy over the whole attractive region of the PES is a key requisite to properly describe weak interaction at room temperature, that is, when there is enough energy in the system to sample a large region of the PES around shallow minima. To achieve these goals, we further require the energy provided by our DFT-SAM model to be not only continuous with respect to the atomic coordinates but also continuously differentiable at least twice so that analytical frequencies can be computed and correct second order information can be used for dynamic simulations.

First, we must construct a density functional that serves as an optimal baseline for the empirical dispersion add-on. In particular, such functional should be characterized by a reduced amount of long-range spurious interactions (which do not decay as R^{-6}) while providing an accurate description of the location and slope of the repulsive energy wall when two atoms become too close. The latter is typically not an issue with many functionals that are accurate enough for thermochemistry and describe correctly minimum energy geometries. Then, we shall develop the SAM for dispersion, which will depend on three quantities for each atom pair: the $C_{6,AB}$ coefficient, a $R_{s,AB}$ *distance offset*, and a damping radius $R_{d,AB}$. These quantities control how the otherwise diverging R^{-6} dispersive interaction gives way to the other forces involved in the chemical bond

Special Issue: Berny Schlegel Festschrift

Received: September 7, 2012
Published: September 28, 2012

   dx.doi.org/10.1021/ct300778e | *J. Chem. Theory Comput.* 2012, 8, 4989−5007

(electrostatic, exchange, correlation, etc.) as the distance between the two atoms decreases. The practical implementation of this new SAM dispersion model hinges on our ability to accurately estimate these three quantities from tables of atomic ionization potentials (IP) and polarizabilities (α), together with a few global parameters.

The idea of designing a *dispersionless* density functional and subsequently adding an empirical dispersion approximation is not new.[32,33] However, in our work, we implement that idea in a more simple and straightforward way in order to preserve the accuracy of the underlying DFT method for those properties for which it has been optimized. Moreover, we maintain the ability to compute analytical energy first and second derivatives using the usual techniques and avoid any increase in computational cost.

The SAM model assumes that intermolecular dispersion interactions are the sum of pairwise spherically symmetric atomic interactions and that the atomic parameters are transferable. These approximations, although far from exact, are common among empirical dispersion models. Our goal is an empirical model whose accuracy is limited as much by these fundamental approximations as by its particular functional form. There are models based on DFT that avoid these limitations,[5−14,34] but these involve either post-SCF (self-consistent field) calculations or six-dimensional numerical quadratures, and hence involve significant increased computation cost for larger systems.

In presenting the conceptual development of our SAM dispersion model, we shall focus on a training set that includes only noble gas dimers and a few small hydrocarbon dimers. We will later apply the model to a variety of diatomic and polyatomic molecules, both polar and nonpolar. The problem of including dispersion forces in density functional theory has received considerable attention in recent years.[5−25,27,28,34] When practical, we shall compare our DFT-SAM model with some of the leading alternatives.

2. FORMULATION OF THE DFT-SAM MODEL

The first step in the development of our model is the definition of a density functional characterized by a minimal amount of spurious long-range interactions that do not decay as R^{-6}. Afterward, we will identify a simple form of empirical dispersion add-on, based on a spherical atom model, and we will optimize the parameters involved.

2.1. APF Functional. We considered all the dimers of the noble gases from He through Xe, together with methane, ethylene, and acetylene dimers. For the methane dimers we considered two conformations of D_{3d} symmetry, corresponding to the C−H···H−C and H−C···C−H interactions, while for the ethylene and acetylene dimers we choose the conformation in which the planes containing the monomers intersect at a right angle. For these systems, we computed the whole potential energy curves at the HF, MP2, and CCSD(T) levels as well as several DFT functionals, both with and without counterpoise (CP) corrections.[35] We use the CCSD(T) method,[36−39] extrapolated to the basis set limit, as our reference for the accurate inclusion of dispersion from first principles.

Since dispersion is a result of electron correlation, it is useful to evaluate the relative error in the correlation energies of weakly bound complexes as a function of distance:

$$\chi_{\text{model}}(R) = \frac{[E_{\text{model}}(R) - E_{\text{model}}(\infty)] - [E_{\text{HF}}(R) - E_{\text{HF}}(\infty)]}{[E_{\text{CCSD(T)}}(R) - E_{\text{CCSD(T)}}(\infty)] - [E_{\text{HF}}(R) - E_{\text{HF}}(\infty)]} \quad (2)$$

At long ranges, $\chi(R)$ is the relative error in the dispersion energy. Near the equilibrium distance, the interaction energy reflects a balance of dispersive attraction, which arises purely from electron correlation, and the Pauli repulsion, which is included in the HF energy but which is reduced slightly when electron correlation, is included. At small R, the primary effect of correlation is to moderate the repulsion slightly.

For HF, $\chi(R) = 0$ for all R and for CCSD(T)/CBS $\chi(R) = 1$. For any model that includes the proper R^{-6} dependence for dispersion, $\chi(R)$ will approach a constant value. Since standard DFT functionals do not include any R^{-6} long-range interactions, they all produce $\chi(R)$ that goes to 0, either from above (spurious attractive interactions at shorter R) or from below (spurious repulsive interactions at shorter R). Our goal is to produce a functional for which $\chi(R)$ is as small in magnitude as possible at intermediate R, in particular, for values of R close to the equilibrium distance. The goal of our work is a combination of DFT and empirical dispersion add-on, where the latter involves a suitable damping function ensuring its contribution would vanish at typical covalent bond distances. Taking a linear combination of well established functionals is clearly a pragmatic way of removing spurious medium- and long-range interactions. An alternative approach would be to modify the form of the functional itself.[32,40] However, the effects of such changes on the performance of the functional for structures and thermochemistry would need to be thoroughly assessed. Following a simpler and more pragmatic approach, we choose a linear combination of functionals to behave properly for the specific type of interaction present in the noble gas and small hydrocarbon dimers, and for the appropriate range of distances.

We examined various density functionals such as B3LYP,[29] B3PW91,[41] PBE1PBE,[42] M05-2X,[43] M06-2X, TPSS,[44] B2PLYP,[45] and mPW2PLYP,[45] and we found that they show medium- to long-range interactions that decay exponentially. In some cases, such interactions are attractive, while in other cases they are repulsive or they correspond to a mixture of attraction and repulsion, depending on the distance. The diverse behavior of such functionals can be appreciated in Figure 1, which reports a plot of the measure defined in eq 2 for the specific case of the Ne dimer, using the aug-cc-pVTZ basis set.

All the functionals considered provide reliable structures and thermochemistry in various test sets. For the systems under consideration, B3PW91 shows consistent repulsive behavior both at intermediate and long distances, while PBE1PBE (also known as PBE0) shows consistent attraction in the same distance range. Therefore, we optimized a combination of 41.1% B3PW91 and 58.9% PBE1PBE that effectively removes all spurious interactions in the Ne dimer. Without any reoptimization, the same combination of functionals works reasonably well for all the other noble gas dimers and also for the small hydrocarbon dimers. In particular, at longer distances, most of the spurious interactions are consistently removed, while they are significantly reduced around the minimum. At shorter distances, they cannot be further reduced, as B3PW91 tends to become attractive for the heavier elements. We call this combination of B3PW91 and PBE1PBE the APF functional. Both B3PW91 and PBE1PBE are hybrid functionals, and their combination in APF results in 23% of Hartree−Fock exchange.

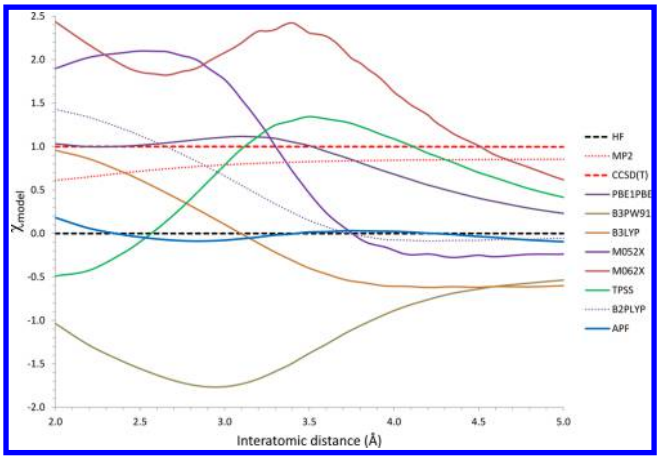

Figure 1. Plot of the χ_{model} as defined in eq 2 for the case of Ne_2. All calculations were carried out using the aug-cc-pVTZ basis set and including the counterpoise correction.

Since both B3PW91 and PBE1PBE have been thoroughly validated for structures and thermochemistry, their straightforward combination in APF can be expected to provide equally reliable structures and thermochemistry, while minimizing long-range spurious interactions. We choose this simple approach rather than attempting a reoptimization of the functional form.[32,33]

2.2. Spherical Atom Model (SAM) for Dispersion. We have developed a spherical atom model (SAM) for dispersion forces as an alternative to the point-multipole expansion. In this model, we evaluate the dispersion interaction between two spherical shells of polarizable material. The thickness of these shells is assumed to be infinitesimal and their radii are $r_{s,A}$ and $r_{s,B}$, respectively. The resulting interatomic potential can be evaluated analytically leading to the following expression:[46]

$$V(R_{AB}) = \frac{C_{6,AB}}{[R_{AB}^2 - (r_{s,A} + r_{s,B})^2]^3} \times \left\{1 - \frac{2}{R_{AB}^2}[r_{s,A}r_{s,B} - (r_{s,A} - r_{s,B})^2] + O(R_{AB}^{-4})\right\} \quad (3)$$

The second term on the right-hand side of eq 3 is numerically much smaller than the first and does not provide a correction to the leading behavior, but rather, it affects only higher terms that are already partially accounted for at large separations. Therefore, we define our SAM potential using only the leading term in eq 3, that is,

$$V^{SAM}(R_{AB}) = \frac{C_{6,AB}}{[R_{AB}^2 - (r_{s,A} + r_{s,B})^2]^3} \quad (4)$$

If this expression is expanded in a Taylor series for R_{AB} large with respect to $r_{s,A} + r_{s,B}$, we obtain

$$V(R_{AB}) \approx \frac{C_{6,AB}}{R_{AB}^6}\left[1 + 3\left(\frac{r_{s,A} + r_{s,B}}{R_{AB}}\right)^2 + 6\left(\frac{r_{s,A} + r_{s,B}}{R_{AB}}\right)^4 + ...\right] \quad (5)$$

This shows that the effective interatomic *distance offset* $R_{s,AB} = r_{s,A} + r_{s,B}$ provided by the finite shell leads to a potential, which contains not only the leading R^{-6} term but also R^{-8} and R^{-10} contributions.

Any expression of this type diverges as R_{AB} becomes small, and in our case, eq 4 diverges as R_{AB} goes to $r_{s,A} + r_{s,B}$. Since these expressions do not describe the interactions at short-range, they are always combined with a suitable damping function.[16,17,47−55] For preliminary testing of the spherical atom potential, we used a simple exponential damping function:

$$V'(R_{AB}) = V(R_{AB})(1 - e^{-\zeta(R_{AB} - R_d)}) \quad (6)$$

We can then compare the resulting potential curves for the argon dimer[56] using various choices for $V(R_{AB})$, each with optimized ζ and R_d:

(a) A point multipole expansion (C_6R^{-6}, $C_6R^{-6} + C_8R^{-8}$, ...) with exact coefficients derived from experimental data.

(b) The SAM potential, with $R_{s,AB}$ computed to give the exact $C_{8,AB}$ value:

$$R_{s,AB} = \sqrt{\frac{C_{8,AB}}{3C_{6,AB}}} \quad (7)$$

(c) The SAM potential with $R_{s,AB}$ as an adjustable parameter rather than fixed to reproduce the exact $C_{8,AB}$.

In case a, an accurate representation of the potential curve requires terms up to C_{10}, along with optimized ζ and R_d. Including only the C_6R^{-6} term with the exact C_6 value produced less than half the net binding energy. Increasing the value of C_6 to produce the correct well depth produces a long-range interaction that is too large by a factor of 2. Therefore, a simple C_6R^{-6} function is not flexible enough to reproduce both the equilibrium binding energy and the binding energy in the long-range.

In case b, we underestimate the binding energy by almost 20%, which is still unacceptable, but is significantly better than what can be achieved including only the C_6R^{-6} term in case a. On the other hand, if we treat $R_{s,AB}$ as an adjustable parameter, as in case c, we can fit the potential energy curve to within the accuracy of CCSD(T) in the Complete Basis Set (CBS) limit.

This example shows how the SAM potential, $V(R; C_6, R_s, \zeta, R_d)$ with a fixed value for C_6, is comparable in accuracy to the point multipole potential, $V(R; C_6, C_8, C_{10}, \zeta, R_d)$, which includes separate values for C_6, C_8, and C_{10}. The additional flexibility provided by the *distance offset* parameter allows the single term with the two parameters of the SAM potential to effectively behave like the first three terms in the point multipole expansion. This suggests that the deviation of the dispersion interaction from the asymptotic C_6R^{-6} behavior arises primarily from the distribution of the induced dipoles over the finite volume of each atom. The interaction among higher-order induced point multipoles appears to be much less important if the point-dipole approximation is relaxed.

2.3. Damping Function. We shall also employ the spherical atom concept in the definition of a new damping function. The attenuation of the Coulomb interaction between a point charge, q_B, at point B, and a 1s orbital with exponent, ζ, on center A, as the charge penetrates the orbital is given by[57]

$$V(R_{AB}) = \frac{q_B}{R_{AB}}[1 - (1 + \zeta R_{AB})\, e^{-2\zeta R_{AB}}] \quad (8)$$

The damping function in an empirical dispersion model should describe the same physical phenomenon, and therefore, the mutual attenuation of two centers will be proportional to the square of the terms in brackets in eq 8. This attenuated Coulomb interaction vanishes at $R_{AB} = 0$, but the SAM dispersion energy diverges at $R_{AB} = R_{s,AB} = r_{s,A} + r_{s,B}$, so we must modify the damping function to vanish at some damping

distance $R_{d,AB} > R_{s,AB}$. The expression for the SAM damping function is thus

$$f(R_{AB}) = \begin{cases} 0 & R_{AB} \le R_{d,AB} \\ \left[1 - \left(1 + 2\frac{R_{AB} - R_{AB}}{R_{d,AB}}\right) \times e^{-4\left(\frac{R_{AB}-R_{d,AB}}{R_{d,AB}}\right)}\right]^2 & R_{AB} > R_{d,AB} \end{cases} \quad (9)$$

This damping function has a strong physical motivation, but its second and higher derivatives with respect to R_{AB} are discontinuous. This may seem a detail, since the energy and first derivative are continuous and that is sufficient to carry out geometry optimization and molecular dynamic simulations. However, the force constants will be affected by this issue and with them the evaluation of the thermal contribution to the free energy. Moreover, any methods for exploring the PES that requires second order information will be affected, too. The most straightforward way to remove such a discontinuity is to multiply $f(R_{AB})$ by a suitable switching function that goes from zero to one with many continuous derivatives. We use a switching function developed for the numerical quadrature in DFT:[58]

$$g(x) = \begin{cases} 0 & x \le -1 \\ \frac{1}{2} + \frac{3003}{2048}\left(\left(\left(\left(\left(\frac{1}{13}x^2 - \frac{6}{11}\right)x^2 + \frac{5}{3}\right)x^2 - \frac{20}{7}\right)x^2 + 3\right)x^2 - 2\right)x^2 + 1\right)x & -1 < x < 1 \\ 1 & x \ge 1 \end{cases} \quad (10)$$

The piecewise function in eq 10 is continuous together with its derivatives up to sixth order. For our purpose, we define the argument of the polynomial to be

$$x = 2\frac{R_{AB} - R_{d,AB}}{0.05R_{d,AB}} - 1 \quad (11)$$

so that the value of $g(R_{AB})$ goes smoothly from one to zero between $R_{d,AB}$ and $1.05 \times R_{d,AB}$. Note that the coefficients in the polynomial are not parameters, but rather, they are fixed by the requirement of continuous derivatives of the piecewise function. Therefore, the damping function in eq 9 effectively depends only on one parameter, $R_{d,AB}$, which, in turn, depends on the atom pair whose dispersive interaction is being damped. We will show below how to estimate $R_{d,AB}$ using quantities that depend only on one atom rather than a pair of atoms.

We are now ready to perform the final assembly of our SAM empirical dispersion potential which assumes the following form:

$$V^{SAM}(R_{AB}) = \begin{cases} 0 & R_{AB} \le R_{d,AB} \\ \frac{C_{6,AB}}{[R_{AB}^2 - R_{s,AB}^2]^3} f(R_{AB}) \times g(R_{AB}) & R_{AB} > R_{d,AB} \end{cases} \quad (12)$$

where $R_{d,AB} > R_{s,AB}$, and the functions $f(R_{AB})$ and $g(R_{AB})$ are defined in eq 9 and eqs 10 and 11, respectively.

3. PARAMETERIZATION OF THE DFT-SAM MODEL

Our proposed SAM model requires the evaluation of $C_{6,AB}$, $R_{s,AB}$, and $R_{d,AB}$ for each pair of elements, from H through Xe. In the following paragraphs, we describe how to estimate each of the above quantities using atomic ionization potentials (IPs) and polarizabilities (α), along with few adjustable parameters.

3.1. Evaluation of $C_{6,AB}$ from Atomic Polarizabilities.

The $C_{6,AB}$ coefficients for the noble gas dimers vary over more than 2 orders of magnitude from He_2 to Xe_2. The second order perturbation expression[59]

$$C_{6,AB}^{(2)} = \frac{3}{2}\left(\frac{\varepsilon_{H,A}\varepsilon_{H,B}}{\varepsilon_{H,A} + \varepsilon_{H,B}}\right)\alpha_A\alpha_B \quad (13)$$

can be used to approximate the $C_{6,AB}$ coefficients, using calculated values of ε_H, that is, the highest occupied molecular orbital (HOMO) energy and α, the isotropic atomic polarizability.

Polarizabilities from *ab initio* calculations are more sensitive to low angular momentum diffuse functions than to high angular momentum basis functions. Therefore, we have calculated the values of ε_H and α for the noble gases at the MP2 level, using a doubly augmented basis set, aug-aug-cc-pVTZ. This basis set is derived from the standard aug-cc-pVTZ by adding a second more diffuse function for each angular momentum type. The exponent of this function is equal to the exponent of the existing diffuse function scaled by the ratio of the existing diffuse exponent to the smallest exponent in the polarization set.

If we apply the formula in eq 13 in the case of the noble gas dimers, using the calculated ε_H and α, we obtain values of $C_{6,AB}$ that are underestimated by roughly the same percentage with respect to the exact ones, as can be seen in Figure 2. Due to the systematic nature of this error, it appears that a single scale factor of 1.18604 can be applied to the result of eq 13 to

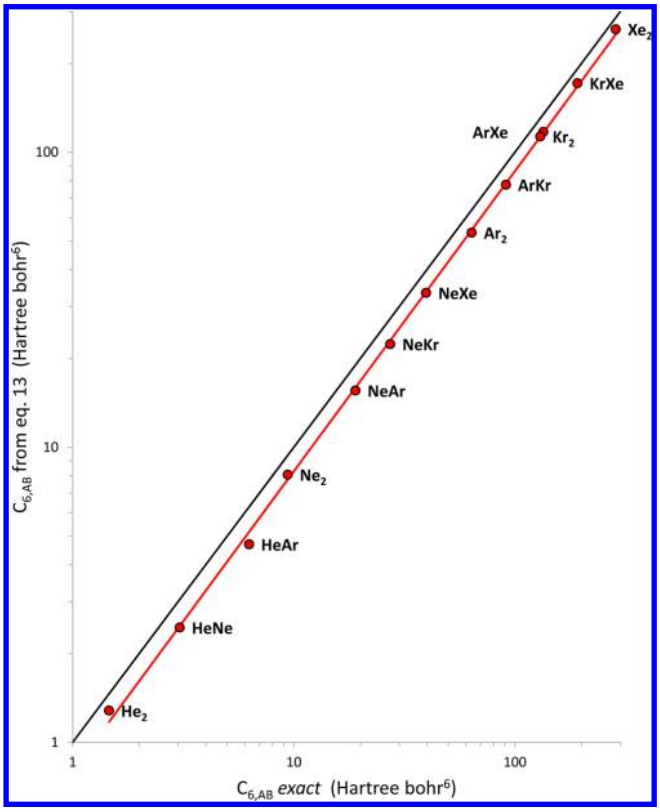

Figure 2. Comparison between the exact $C_{6,AB}$ coefficients of several noble gas dimers and the ones estimated by eq 13 using ε_H and atomic polarizabilities computed at the MP2/aug-aug-cc-pVTZ level.

dx.doi.org/10.1021/ct300778e | J. Chem. Theory Comput. 2012, 8, 4989−5007

reproduce the exact $C_{6,AB}$ coefficients from the MP2 polarizabilities.

3.2. Definition of the Effective Atomic Polarizabilities. The polarizability of a given atom is influenced by the molecular environment that surrounds it. The polarizabilities of isolated open shell atoms (particularly those with partially occupied valence shell AOs) are typically much larger than the contributions that these atoms make to the polarizabilities of molecules. For example, the polarizability of an isolated H atom (α_H = 4.507 bohr^3) is almost twice the contribution of each of the atoms to the polarizability of the H_2 molecule ($\alpha_{H2}/2$ = 5.256/2 = 2.628 bohr^3).

The values of α to be used in calculation of the $C_{6,AB}$ coefficients need to represent different possible bonding situations. There is no unique procedure to partition the polarizability of small molecules into atomic contributions. However, in many cases, the effect of different molecular environments can be reasonably approximated by using a single effective polarizability value for each element.

We computed the polarizability of small molecules at the MP2/aug-aug-cc-pVTZ level and defined the molecular polarizability simply as the sum of atomic contributions,

$$\alpha_{\text{molecule}} = \sum_i \alpha_{Z_i} \tag{14}$$

where the sum runs over all the atoms in the molecule and α_Z is the effective isotropic polarizability of the element with atomic number Z.

First, we adjusted the values of α for hydrogen and carbon in order to reproduce the isotropic molecular MP2/aug-aug-cc-pVTZ polarizabilities of methane, ethane, ethylene, and ethyne with less than 10% relative error. The atomic polarizability of oxygen was then chosen considering a group of molecules including water, carbon monoxide, molecular oxygen, and formaldehyde. Using the values for H, C, and O, the polarizabilitities of nitrogen and fluorine were adjusted separately to reproduce NH_3, NO, formamide, F_2, and HF. The value of α for each remaining main group element was similarly set using the halide, oxide, and hydride for the electropositive elements, or the diatomic and the hydride for the electronegative ones. In most cases, we were able to limit the relative error to 20%. In the case of the alkali, alkaline, and first row transition metals, the cation was included in the test set rather than the more polarizable neutral atom, together with the hydride, fluoride, and oxide. The polarizabilities of the elements in the fourth row of the periodic table (with the exception of iodine) were determined using the computed α of the cations scaled by the ratio between the effective and computed polarizabilities of a corresponding third row species. In the case of iodine, the diatomic molecule and the hydride were used to fix the value of α. For the atomic polarizability of the noble gas elements the MP2/aug-aug-cc-pVTZ values were used.

In Table 1, we collect the computed values of the ionization potential (ε_H, Koopman's Theorem ionization potentials) for elements H through Xe, while in Table 2 the effective atomic polarizabilities used in our model are reported. The ionization potential (IP) values of H, C, and Be required special consideration. In the case of Be, we use the CCSD(T) value of the IP, since the near degeneracy of the 2s and 2p orbitals leads to an unacceptable error at the SCF level. Moreover, rather than using the atomic IP for H and C, we use the corresponding values for the diatomics H_2 and C_2. This reflects

Table 1. Ionization Potentials, Defined as $-\varepsilon_H$ of the Elements H through Xe as Computed at the HF/aug-aug-cc-pVTZ Level (See Text for Details)

1																2	
H_2																He	
0.593																0.918	
3	4											5	6	7	8	9	10
Li	Be											B	C_2	N	O	F	Ne
2.487	0.836											0.318	0.456	0.571	0.678	0.77	0.851
11	12											13	14	15	16	17	18
Na	Mg											Al	Si	P	S	Cl	Ar
1.519	0.319											0.218	0.301	0.373	0.416	0.446	0.591
19	20	21	22	23	24	25	26	27	28	29	30	31	32	33	34	35	36
K	Ca	Sc^+	Ti^+	V^+	Cr^+	Mn^+	Fe^+	Co^+	Ni^+	Cu	Zn	Ga	Ge	As	Se	Br	Kr
0.956	0.288	0.487	0.634	0.717	0.792	0.868	0.918	0.955	0.988	1.501	0.293	0.215	0.291	0.342	0.384	0.435	0.524
37	38	39	40	41	42	43	44	45	46	47	48	49	50	51	52	53	54
Rb	Sr	Y^+	Zr^+	Nb^+	Mo^+	Tc^+	Ru^+	Rh^+	Pd^+	Ag	Cd	In	Sn	Sb	Te	I	Xe
0.81	0.258	0.436	0.533	0.608	0.61	0.759	0.89	0.846	0.869	1.382	0.265	0.197	0.265	0.294	0.317	0.364	0.458

dx.doi.org/10.1021/ct300778e | J. Chem. Theory Comput. 2012, 8, 4989−5007

Table 2. Effective Atomic Polarizabilities (a.u.) of the Elements H through Xe[a]

1																	2
H																	He
1.904																	1.364
3	4											5	6	7	8	9	10
Li	Be											B	C	N	O	F	Ne
0.484	7.316											9.24	8.782	5.613	4.833	3.249	2.711
11	12											13	14	15	16	17	18
Na	Mg											Al	Si	P	S	Cl	Ar
2.011	15.028											14.679	21.355	23.829	19.802	15.047	10.97
19	20	21	22	23	24	25	26	27	28	29	30	31	32	33	34	35	36
K	Ca	Sc	Ti	V	Cr	Mn	Fe	Co	Ni	Cu	Zn	Ga	Ge	As	Se	Br	Kr
12.722	15.195	15.734	27.922	16.137	22.125	24.567	19.602	17.982	17.24	5.015	19.29	23.448	22.399	29.659	26.008	21.558	16.959
37	38	39	40	41	42	43	44	45	46	47	48	49	50	51	52	53	54
Rb	Sr	Y	Zr	Nb	Mo	Tc	Ru	Rh	Pd	Ag	Cd	In	Sn	Sb	Te	I	Xe
15.648	18.69	19.353	34.344	19.848	27.214	30.218	24.11	22.118	21.205	7.567	23.726	29.388	30.128	41.938	38.52	33.951	27.577

[a]These values have been chosen to reproduce molecular polarizabilities computed at the MP2/aug-aug-cc-pVTZ level (see text for more details).

the contraction of the orbitals of C and H upon forming bonds, and the associated lowering of the orbital energy.

In both tables, it is possible to identify simple patterns. For a fixed valence shell configuration, the IPs decrease and the polarizabilities increase with increasing principal quantum number. The nonmetals (groups III through VIII) show similar systematic behavior. The IPs increase almost monotonically as a given valence shell becomes filled, while the polarizabilities typically increase with the principal quantum number and show rather regular patterns as a given shell is filled. In Figure 3, we show how the molecular polarizability of many small molecules can be well reproduced using the values in Table 2.

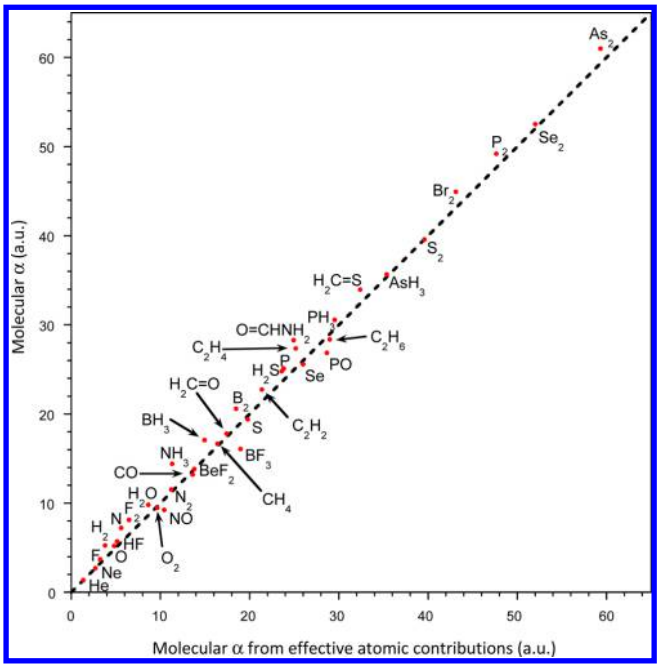

Figure 3. Comparison between molecular polarizabilities of several small molecules computed at the MP2/aug-aug-cc-pVTZ level and values estimated from atomic contributions using the effective atomic polarizabilities in Table 2.

3.3. Relation between $R_{s,AB}$ and $R_{d,AB}$ and Atomic Radii and Ionization Potentials. The determination of specific $R_{s,AB}$ and $R_{d,AB}$ values for each pair of elements would greatly increase the number of parameters required by our model. The ultimate purpose of $R_{s,AB}$ and $R_{d,AB}$ is to modify and attenuate the R_{AB}^{-6} dispersion term in the region of space where the electron densities of adjacent atoms begin to overlap. At large distances, the radial part of any atomic orbital decays exponentially[60] as

$$\varphi(r) \sim e^{-\sqrt{-\varepsilon_H} r} \tag{15}$$

and since the HOMO is related to the density distribution of the outer electrons, which are the ones most involved in the dispersion interaction, it provides a suitable definition of a distance at which an empirical model of such interaction should be damped. In fact, since a measure of an effective "atomic radius" can generally be defined to be inversely proportional to the square root of $-\varepsilon_H$, that is,

$$R \sim \frac{1}{\sqrt{-\varepsilon_H}} \tag{16}$$

we can postulate the existence of relationships that will provide $R_{s,AB}$ and $R_{d,AB}$ given $\varepsilon_{H,A}$ and $\varepsilon_{H,B}$. In particular, we will model both $R_{s,AB}$ and $R_{d,AB}$ using a linear dependence upon the inverse square root of the average of $\varepsilon_{H,A}$ and $\varepsilon_{H,B}$,

$$R \sim p\frac{1}{\sqrt{-\left(\frac{\varepsilon_{H,A}+\varepsilon_{H,B}}{2}\right)}} + q \tag{17}$$

For comparison, optimized values of $R_{s,AB}$ and $R_{d,AB}$ were obtained for all noble gas dimers by least-squares fitting of the CCSD(T)/CBS potential energy curves using basis set extrapolated APF energies augmented by the SAM empirical dispersion as in eq 12, where the values of $C_{6,AB}$ were estimated as described in section 3.1.

In Figure 4 are reported the optimized values of $R_{s,AB}$ for all the noble gas dimers. Two distinct linear trends can be identified according to whether a helium atom is present. Both linear trends can be constrained to go through the origin without significant loss of accuracy. The optimized values of $R_{d,AB}$ are collected in Figure 5 where a single linear dependence is observed for all noble gas dimers. This confirms the hypothesis of a linear relationship of $R_{s,AB}$ and $R_{d,AB}$ with the inverse square root of $-\varepsilon_H$.

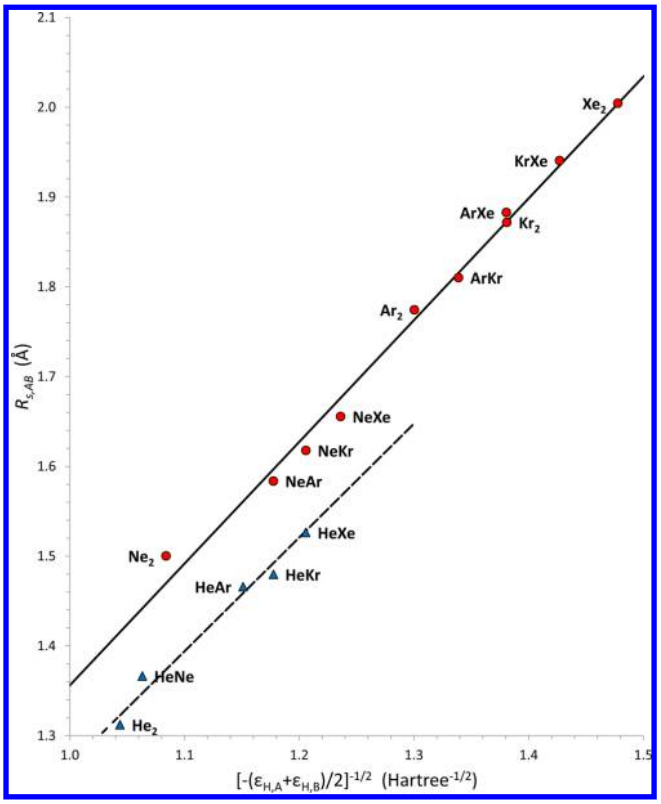

Figure 4. Plot of the optimized values of $R_{s,AB}$ for several noble gas dimers and the two linear trends described in Table 3.

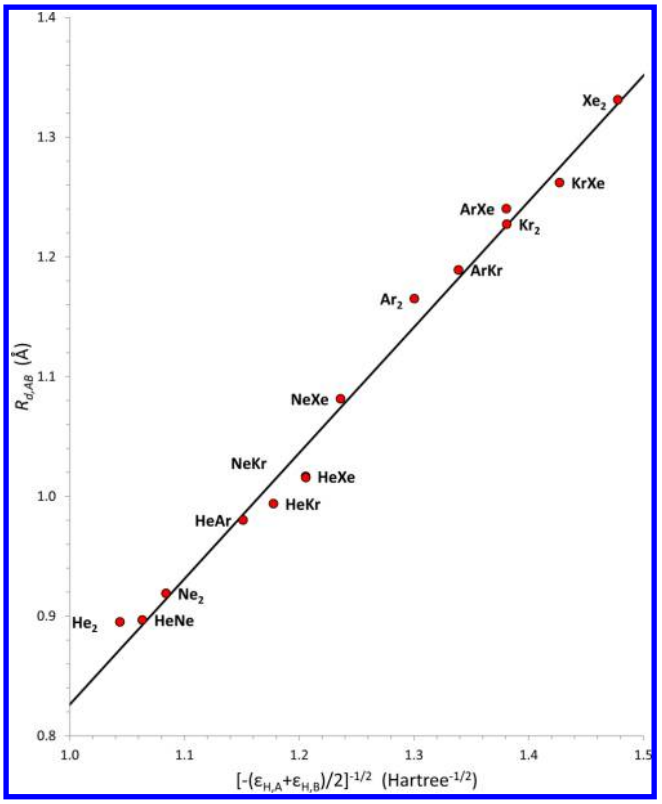

Figure 5. Plot of the optimized values of $R_{d,AB}$ for several noble gas dimers and the linear trend described in Table 3.

3.4. Final Parameter Specifications. Up to this point, the training set for the parametrization of our empirical dispersion model has been limited to the 15 noble gas dimers. However, further adjustments are required to handle interactions involving hydrogen and carbon, and therefore, we extended our training set by including the same four hydrocarbon dimers used in the definition of the APF functional.

In Table 3, we present the full parametrization of APF-D. In the case of $R_{s,AB}$, a simple scaling of the inverse square root of the average of $\varepsilon_{H,A}$ and $\varepsilon_{H,B}$ is required, while for $R_{d,AB}$, a uniform shift is also needed. These two linear relationships and the additional adjustments required when helium, hydrogen, or carbon are involved altogether depend on eight parameters. Therefore, the empirical dispersion model in APF-D depends

Table 3. Parameterization of the Empirical Dispersion Model in APF-D

$$E_{disp} = \sum_{A>B} V^{SAM}(R_{AB}) \quad V^{SAM}(R_{AB}) \text{ from eq 12}$$

$$C_{6,AB} = \frac{3}{2}P_1\left(\frac{\varepsilon_{H,A}\varepsilon_{H,B}}{\varepsilon_{H,A}+\varepsilon_{H,B}}\right)\alpha_A\alpha_B \quad P_1 = 1.18604$$

$$R_{s,AB} = \frac{P_i}{\sqrt{-\frac{1}{2}(\varepsilon_{H,A}+\varepsilon_{H,B})}}$$

$$P_i = \begin{cases} P_2 = 1.356477 \times 0.933949, & \text{if AB = HH or XHe} \\ P_3 = 1.356477 \times 0.396997, & \text{if AB = CH} \\ P_4 = 1.356477 \times 0.793994, & \text{if AB = XH, X} \neq \text{C} \\ P_5 = 1.356477, & \text{otherwise} \end{cases}$$

$$R_{d,AB} = \frac{P_j}{\sqrt{-\frac{1}{2}(\varepsilon_{H,A}+\varepsilon_{H,B})}} - P_6 \quad P_6 = 0.234859$$

$$P_j = \begin{cases} P_7 = 1.058675 \times 0.793994, & \text{if AB = CH} \\ P_8 = 1.058675 \times 0.933949, & \text{if AB = XH, X} \neq \text{C} \\ P_9 = 1.058675, & \text{otherwise} \end{cases}$$

dx.doi.org/10.1021/ct300778e | J. Chem. Theory Comput. 2012, 8, 4989−5007

on two atomic properties (ε_H and effective atomic polarizability) and a total of nine parameters.

This is sufficient to reproduce the whole potential energy curves of the 19 systems in the training set. The accuracy of APF-D in the case of the noble gas dimers is apparent in Figure 6, where the root-mean-square error rarely exceeds 10 cal mol^{-1}

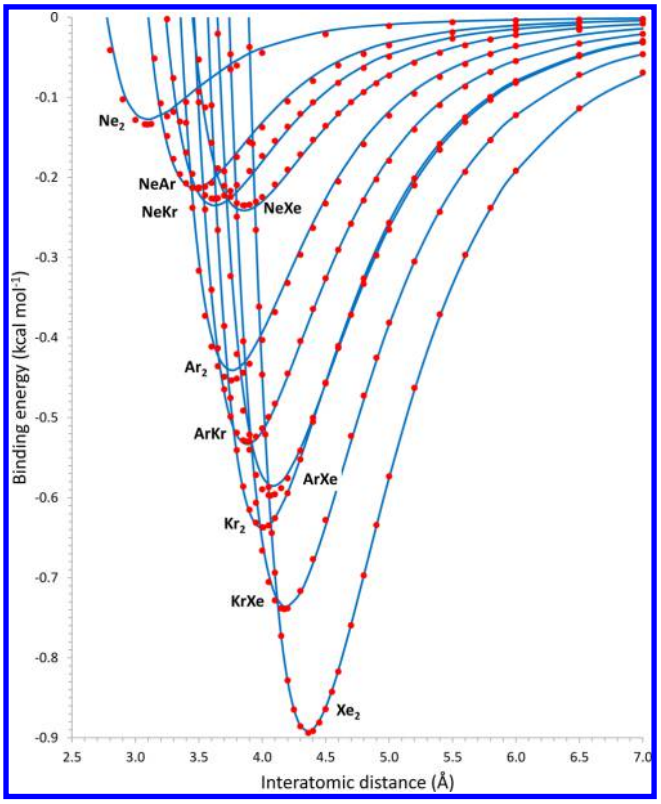

Figure 6. Comparison between the potential energy surface of several noble gas dimers as computed by CCSD(T) (red dots) and APF-D (blue lines). The results of both methods have been extrapolated to the complete basis set limit.

over a region including the minimum and extending all the way to the dissociation limit. Similar accuracy is achieved for the four hydrocarbon dimers over the corresponding range of distances as can be seen in Figure 7. Note that the dispersion model in APF-D is flexible enough to reproduce the interaction curves of the hydrocarbon dimers without any specific adjustment for different hybridization states of the carbon atom.

4. RESULTS AND DISCUSSION

Despite the number of benchmark data sets of weak interactions that have been published in recent years, it appears that no single standard has emerged. Moreover, these data sets may be affected by shortcomings such as the lack of a proper extrapolation of the reference energies to the complete basis set limit, an inconsistent choice of the monomer geometries and the preferential focus on one specific point (the minimum) on the potential energy surface. On the other hand, numerous methods to accurately describe weak interactions have been published in the literature. Most of these methods involve a significant amount of parametrization or a large data set for interpolating the parameters involved in the dispersion model.

In this section, we explore the performance of the APF-D/aug-cc-pVTZ model on a variety of weakly bound species and

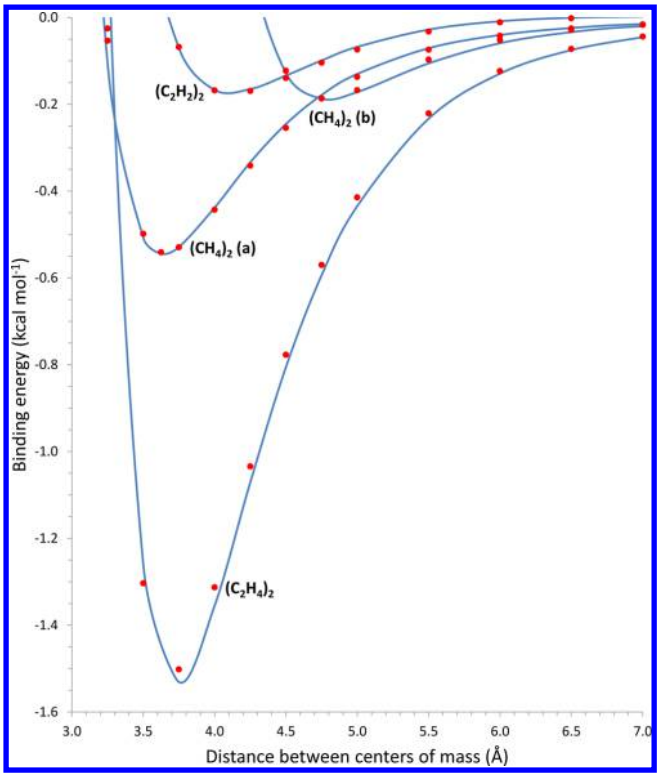

Figure 7. Comparison between the interaction energy profiles of four dimers of small hydrocarbons as computed by CCSD(T) (red dots) and APF D (blue lines). The results of both methods have been extrapolated to the complete basis set limit. For the methane dimer the (a) conformation corresponds to the H−C···C−H interaction, while the (b) conformation corresponds to the C−H···H−C interaction. For the ethylene and acetylene dimers the planes containing the monomers intersect at a right angle.

also on conformational energy differences. We will include in our results what we believe is a considerate choice of systems representative of different types of weak interactions (both inter- and intramolecular dispersive interactions, hydrogen bonding, and weak covalent bonds). Some of these systems are already included in published benchmark data sets. In addition, we will consider also strong covalent and ionic bonds to confirm that APF-D provides accurate results across the board. We will assess the accuracy of the APF-D results and other methods with CCSD(T)/CBS or with experimental results where practical. We will compare the accuracy of APF-D in describing weak interactions against three other methods: (a) the M05-2X functional, which does not include an empirical dispersion add-on but nevertheless has been rather successful in reproducing intermolecular interaction energies; (b) the B97-D3 functional,[61] which has been reparameterized[18] together with an empirical dispersion term; and (c) the B2PLYP-D3 double hybrid method, which involves both a second order perturbative correction to the SCF energy and an empirical dispersion term. Note that the cost of a B2PLYP-D3 calculation may be significantly larger than that of M05-2X, B97-D3 or APF-D.

Since counterpoise (CP) corrections are not well-defined for intramolecular interactions and may be included in the parametrization of the empirical dispersion model, we will explicitly measure their effect when practical by comparing results with and without such corrections. All calculations have

Table 4. Calculated and Experimental Bond Lengths (in Å) of the Noble Gas Dimers[a]

	M05-2X	B97-D3	B2PLYP-D3	APF-D	APF-D CP	MP2	CCSD(T)	exp.	ref
He···He	2.751	3.003	2.784	2.933	2.936	3.105	3.015	2.97	73
He···Ne	2.794	3.166	2.914	3.029	3.057	3.089	3.033	3.031	74
Ne···Ne	2.875	3.339	3.006	3.101	3.151	3.163	3.107	3.091	73
He···Ar	3.309	3.672	3.521	3.465	3.482	3.542	3.505	3.48	74
Ne···Ar	3.332	3.747	3.443	3.451	3.475	3.544	3.518	3.489	74
Ne···Kr	3.515	3.886	3.592	3.612	3.633	3.741	3.717	3.621	74
He···Kr	3.531	3.831	3.687	3.658	3.667	3.775	3.741	3.693	74
Ar···Ar	3.769	4.005	3.761	3.733	3.75	3.766	3.814	3.757	73
Ne···Xe	3.741	4.11	3.85	3.824	3.866	4.001	3.977	3.861	74
Ar···Kr	3.941	4.095	3.887	3.87	3.88	3.926	3.982	3.881	74
He···Xe	3.786	4.115	4.148	3.948	3.984	4.105	4.066	3.978	74
Kr···Kr	4.112	4.18	4.007	3.996	4.001	4.073	4.136	4.008	73
Ar···Xe	4.148	4.262	4.106	4.05	4.074	4.138	4.201	4.067	74
Kr···Xe	4.306	4.334	4.215	4.165	4.184	4.271	4.343	4.174	74
Xe···Xe	4.493	4.482	4.419	4.324	4.355	4.462	4.541	4.363	73
RMS error	0.152	0.195	0.08	0.025	0.021	0.09	0.098		

[a]All calculations were performed using the aug-cc-pCVTZ basis sets.[62,63] CP corrections were not applied unless explicitly stated.

Table 5. Calculated and Experimental Dissociation Energies (in cal mol^{-1}) of the Noble Gas Dimers[a]

	M05-2X	B97-D3	B2PLYP-D3	PW86PBE XDM[b]	APF-D	APF-D CP	MP2	CCSD(T)	CCSD(T) CBS[c]	exp.	ref
He···He	24.8	51.3	21.4	18	23.5	22.7	14.0	19.6	20.6	21.8	73
He···Ne	83.7	80.1	60.1	48	50.6	41.0	42.2	56.0	41.0	41.1	74
Ne···Ne	181.0	113.1	109.7	100	92.2	72.7	82.7	108	83.0	84.0	73
He···Ar	84.9	82.4	42.7	59	59.9	55.0	55.4	62.2	57.8	57.5	74
Ne···Ar	200.4	144.2	125.9	143	145.3	128.4	129.0	142.7	133.1	134.3	74
Ne···Kr	197.5	163.6	154.9	164	159.3	144.7	130.0	142.8	149.2	142.2	74
He···Kr	79.0	88.4	52.8	65	61.6	58.7	52.4	58.6	60.8	57.2	74
Ar···Ar	266.4	234.9	229.5	255	291.2	271.0	317.4	272.1	272.8	284.6	73
Ne···Xe	207.9	179.3	144.2		151.1	126.6	136.5	148.8	154.0	147.5	74
Ar···Kr	271.3	294.5	313.9	311	343.6	327.0	356.9	300.3	333.3	361.1	74
He···Xe	81.0	94.8	38.0		62.0	52.0	54.5	60.0	61.5	54.3	74
Kr···Kr	277.6	381.9	434.6	381	410.6	400.0	413.5	341.5	416.9	399.8	73
Ar···Xe	310.1	356.4	338.2		404.6	365.4	413.5	342.9	371.8	374.8	74
Kr···Xe	324.8	481.2	489.4		498.3	461.8	496.2	403.7	480.3	464.0	74
Xe···Xe	386.0	629.0	575.1		626.5	553.7	612.6	491.3	563.6	561.0	73
RMS error	82.4	37.0	26.4	21.6	22.3	11.9	21.4	34.3	10.5		

[a]All calculations were performed using the aug-cc-pCVTZ basis sets[62,63] except of course the estimated CCSD(T)/CBS limit. [b]Ref 75. [c]CCSD(T)/CBS//APF-D/aug-cc-pVTZ with CCSD(T) including 3d electrons on Kr and 4d electrons on Xe.

been carried out with the development version of the Gaussian system of programs.

4.1. Noble Gas Dimers. In Tables 4 and 5 are collected the predicted equilibrium distances and binding energies for 15 noble gas dimers as computed by various methods. For these systems, accurate experimental data are available and they represent our benchmark.

The CCSD(T) calculations require a larger aug-cc-pCVTZ basis sets[62,63] and inclusion of the Kr 3d and Xe 4d electrons to achieve a high level of accuracy on the equilibrium distances. However, the binding energies show good accuracy with just the aug-cc-pVTZ basis excluding correlation of the d-electrons. It is easy to extrapolate the CCSD(T)/aug-cc-pCVQZ//APF-D/aug-cc-pVTZ energies to the CBS limit by adding the difference between the aug-cc-pCVQZ[62,63] energy and the one obtained with the corresponding triple-ζ basis set. The RMS error vs experiment is reduced to 10 cal mol^{-1} in the binding energies, and the difference between the CCSD(T) energies with and without CP corrections is also reduced to 3 cal mol^{-1}.

The APF-D/aug-cc-pVTZ model delivers an RMS error as low as 0.025 Å for the equilibrium distances. The basis set superposition error (BSSE) from this modest basis set leads to bond lengths that are on the average 0.021 Å too short. Including the CP corrections for the BSSE results in bond lengths that are on average too long by only 0.004 Å, but it has little effect on the overall RMS error. The accuracy of APF-D on the binding energy is comparable to that of CCSD(T)/CBS. The noble gas dimers are the conceptual basis for the spherical atom model,and they constitute the bulk of the training set used to parametrize our empirical dispersion. Therefore, extremely accurate results on the noble gas dimers are to be expected, and they can be considered a measure of the limitations of the model.

Zhao and Truhlar have evaluated[64] the performance of 18 functionals for weakly bound complexes, and they found the best mean absolute deviation (MAD) for the bond lengths of the noble gas dimers to be 0.14 Å. According to our calculations, the M05-2X/aug-cc-pVTZ method provides an RMS error of 0.152 Å on the equilibrium distances and 82.4 cal

Table 6. Minimum Energy Distances (in Å) of Argon Complexes with Nonpolar Molecules[a]

	M05-2X	B97-D3	B2PLYP-D3	APF-D	APF-D CP	MP2	CCSD(T)	CCSD(T) CP	CCSD(T) CBS	literature	ref
Ar···H_2 ⊥	3.526	3.772	3.568	3.649	3.686	3.588	3.572	3.673	3.577	3.582	76
Ar···H_2 ∥	3.530	3.631	3.458	3.650	3.694	3.531	3.528	3.682	3.619	3.617	76
Ar···Be	4.253	3.937	4.222	4.134	4.172	4.231	4.279	4.375	4.263	4.232	
Ar···B_2 ⊥	3.653	3.602	3.810	4.048	4.077	3.807	3.957	4.065	3.956		
Ar···B_2 ∥	4.600	4.499	4.435	4.667	4.718	4.440	4.624	4.779	4.684		
Ar···CH_4	3.685	3.810	3.656	3.683	3.697	3.640	3.655	3.739	3.668	3.704	77
Ar···H−CH	4.217	4.261	4.099	4.210	4.239	4.135	4.136	4.290	4.234		
Ar···HCCH ⊥	3.863	4.028	3.848	3.820	3.839	3.789	3.876	3.958	3.873		
Ar···HCCH ∥	4.626	4.564	4.487	4.589	4.628	4.476	4.490	4.669	4.623		
Ar···N_2 ⊥	3.674	3.905	3.675	3.685	3.723	3.608	3.670	3.791	3.723	3.711	78
Ar···N_2 ∥	4.251	4.503	4.185	4.267	4.315	4.167	4.198	4.321	4.262	4.330	78
Ar···O_2 ⊥	3.503	3.837	3.502	3.445	3.473	3.457	3.524	3.611	3.529	3.550	79
Ar···O_2 ∥	4.032	4.377	3.987	4.036	4.051	3.981	4.021	4.117	4.039	4.020	79
Ar···F_2 ⊥	3.309	3.877	3.431	3.409	3.421	3.426	3.420	3.495	3.416	3.440	80
Ar···F_2 ∥	3.867	4.165	3.784	3.792	3.808	3.805	3.872	3.951	3.867	3.880	80
Ar···Mg	4.516	4.108	4.434	4.634	4.674	4.623	4.672	4.750	4.620		
Ar···SiH_4	3.800	3.929	3.797	3.844	3.871	3.766	3.792	3.893	3.783	3.858	80
Ar···P_2 ⊥	4.106	4.134	4.091	4.001	4.018	4.002	4.152	4.239	4.136	4.136	80
Ar···P_2 ∥	5.031	5.051	4.936	4.940	4.966	4.906	4.991	5.107	5.007		
Ar···SH	3.545	3.574	3.684	3.606	3.622	3.748	3.788	3.849	3.701	3.678	81
∠ HS···Ar	73.10°	77.39	65.58°	69.50°	68.75°	61.17°	60.40°	64.81°	61.85°	66.60°	
Ar···Cl_2 ⊥	3.700	3.813	3.636	3.636	3.659	3.618	3.680	3.770	3.653	3.680	82
Ar···Cl_2 ∥	4.438	4.641	4.448	4.422	4.432	4.386	4.469	4.530	4.380	4.450	82
Ar···Br_2 ⊥	3.837	3.904	3.732	3.712	3.721	3.697	3.768	3.901	3.745	3.800	83
Ar···Br_2 ∥	4.682	4.832	4.692	4.580	4.590	4.572	4.665	4.764	4.616	4.630	83
RMS error	0.087	0.243	0.096	0.061	0.061	0.091	0.054	0.103	0.037		

[a]The distance (in Å) between the argon atom and the center of mass of the nonpolar molecule is optimized while the geometry of the molecule is held fixed (see the Supporting Information for details). All calculations were performed using the aug-cc-pVTZ basis set. CP corrections or CBS extrapolation were not performed unless explicitly stated. RMS errors are computed with respect to CCSD(T)/CBS and the error of CCSD(T)/CBS with respect to the available experimental values is also reported.

mol^{-1} on the binding energies. The accuracy of the M05-2X results on equilibrium geometries and energies is rather remarkable since this functional has no term that gives an explicit R^{-6} attraction. In fact, at long-range the interaction energy from M05-2X goes to zero exponentially rather than as R^{-6}.

In addition to M05-2X, we included in Tables 4 and 5 the results of B97-D3, B2PLYP-D3, MP2, and CCSD(T) using the aug-cc-pVTZ basis set. For the binding energies, we also report the results obtained by Kannemann and Becke using the PW86PBE-XDM(BR) method.[11] The accuracy of both B2PLYP-D3 and PW86PBE-XDM(BR) in predicting the binding energies of the noble gas dimers is comparable to that of APF-D without CP corrections. While both these methods are formally more complex and than APF-D, they differ in their computational cost, since B2PLYP-D3 is more expensive than both APF-D and PW86PBE-XDM(BR).

4.2. Ar···Nonpolar Complexes. As we expand our horizons beyond noble gas dimers, rather than choosing one of the many benchmark data sets of weakly bound complexes, we carefully select smaller sets of systems for which very accurate reference data are available and that provide a significant cross section of many possible kinds of weak interactions.

Argon complexes with nonpolar species provide a consistent a sampling of the periodic table. We choose 24 of such systems (see Supporting Information for more details), and we collected the results of both equilibrium distances and binding energies in Tables 6 and 7. We have performed extrapolation of CCSD(T)/aug-cc-pVTZ and CCSD(T)/aug-cc-pVQZ results to estimate the CBS limit, according to

$$E_{\mathrm{CCSD(T)/CBS}} = E_{\mathrm{CCSD(T)/aug\text{-}cc\text{-}pVQZ}} + \lambda[E_{\mathrm{CCSD(T)/aug\text{-}cc\text{-}pVQZ}} - E_{\mathrm{CCSD(T)/aug\text{-}cc\text{-}pVTZ}}] \quad (18)$$

where λ was adjusted (generally between 0.75 and 0.85) to obtain agreement between extrapolation with and without CP corrections. The same kind of extrapolation has been applied to the equilibrium distances, and the CCSD(T)/CBS extrapolated geometries agree with the accurate values available from the literature to within ±0.038 Å, so that either reference set would be adequate for comparison. However, in both Table 6 and Table 7, we report RMS errors with respect to CCSD(T)/CBS because these results are available for the whole set of 24 systems. The CCSD(T)/aug-cc-pVTZ errors in the binding energies are the most systematic: the binding energy is consistently overestimated before the CP correction and underestimated after the CP correction is included.

The APF-D geometries, with or without CP corrections, are comparable in accuracy to the CCSD(T)/aug-cc-pVTZ geometries, which entail a computational effort several orders-of-magnitude greater. This supports the hypothesis that the simple rules for estimating $C_{6,AB}$, $R_{s,AB}$, and $R_{d,AB}$ that we optimized looking at the noble gas dimers are transferable to other elements using the IPs and effective polarizabilities listed in Tables 1 and 2. Both B2PLYP-D3 and M05-2X are overall slightly less accurate. M05-2X shows a remarkable accuracy in predicting the equilibrium distance, and it is only slightly less

Table 7. Binding Energies (in kcal mol^{-1}) of Argon Complexes with Nonpolar Molecules[a]

	M05-2X	B97-D3	B2PLYP-D3	APF-D	APF-D CP	MP2	CCSD(T)	CCSD(T) CP	CCSD(T)/CBS
Ar···H_2 ⊥	0.141	0.157	0.144	0.093	0.084	0.143	0.149	0.103	0.132
Ar···H_2 ∥	0.172	0.213	0.209	0.130	0.106	0.230	0.232	0.129	0.153
Ar···Be	0.174	0.351	0.193	0.124	0.103	0.253	0.207	0.146	0.176
Ar···B_2 ⊥	0.600	0.667	0.422	0.188	0.164	0.564	0.381	0.268	0.333
Ar···B_2 ∥	0.310	0.393	0.412	0.174	0.139	0.621	0.356	0.223	0.262
Ar···CH_4	0.427	0.390	0.476	0.429	0.392	0.529	0.508	0.346	0.412
Ar···H−CH_3	0.207	0.310	0.356	0.276	0.237	0.387	0.385	0.221	0.255
Ar···HCCH ⊥	0.324	0.313	0.355	0.381	0.352	0.481	0.381	0.275	0.336
Ar···HCCH ∥	0.310	0.507	0.544	0.401	0.332	0.607	0.574	0.295	0.340
Ar···N_2 ⊥	0.288	0.288	0.293	0.291	0.262	0.416	0.334	0.232	0.278
Ar···N_2 ∥	0.196	0.201	0.243	0.191	0.163	0.356	0.314	0.182	0.211
Ar···O_2 ⊥	0.371	0.250	0.301	0.396	0.364	0.424	0.362	0.261	0.336
Ar···O_2 ∥	0.237	0.197	0.276	0.273	0.246	0.398	0.348	0.225	0.276
Ar···F_2 ⊥	0.436	0.215	0.273	0.304	0.272	0.336	0.361	0.251	0.337
Ar···F_2 ∥	0.394	0.243	0.411	0.368	0.332	0.509	0.417	0.277	0.364
Ar···Mg	0.174	0.478	0.232	0.096	0.076	0.227	0.196	0.144	0.193
Ar···SiH_4	0.621	0.576	0.645	0.471	0.418	0.692	0.658	0.450	0.546
Ar···P_2 ⊥	0.363	0.465	0.429	0.537	0.499	0.658	0.442	0.328	0.407
Ar···P_2 ∥	0.254	0.345	0.346	0.367	0.332	0.509	0.395	0.270	0.328
Ar···SH	0.786	0.807	0.513	0.595	0.555	0.536	0.473	0.343	0.467
Ar···Cl_2 ⊥	0.626	0.506	0.601	0.652	0.604	0.787	0.642	0.485	0.624
Ar···Cl_2 ∥	0.548	0.533	0.658	0.633	0.591	0.841	0.664	0.486	0.674
Ar···Br_2 ⊥	0.625	0.629	0.751	0.780	0.737	1.061	0.865	0.518	0.699
Ar···Br_2 ∥	0.632	0.686	0.837	0.861	0.813	1.188	0.935	0.556	0.775
RMS error	0.102	0.142	0.071	0.068	0.071	0.192	0.090	0.095	

[a]All calculations were performed using the aug-cc-pVTZ basis set. CP corrections or CBS extrapolation were not performed unless explicitly stated. The RMS error with respect to CCSD(T)/CBS are reported.

accurate than both APF-D and B2PLYP-D3 for the binding energies. The overall accuracy of the APF-D functional is almost identical to B2PLYP-D3 in Table 7, but the relative accuracy of these models varies from case to case and with the inclusion or omission of CP corrections. B97-D3 does not appear to be competitive for these systems, and while the MP2 geometries are satisfactory, the corresponding binding energies show the largest RMS error.

The weakly bound Ar complexes provide an opportunity to measure deviations from our empirical dispersion model due to the fact that atoms in molecules are no longer spherically symmetric. We can measure the size and shape of an atom in a weakly bound complex either considering the distance at which the repulsive wall in the SCF energy appears, or the position and depth of the attractive well due to dispersive interactions. If atoms in molecules were indeed spherical, we would expect the repulsive wall to appear at the same distance regardless of the direction of approach of the two moieties, and the depth of the attractive well to be roughly proportional to the number of nearest neighbor interactions. Thus, the "T-shaped" C_{2v} structure for the Ar···N_2 complex should be bound almost twice as strongly as the linear structure, and the repulsive walls should be located at the same distance, just as our SAM model predicts and is shown in Figure 8. Indeed, the repulsive walls line up almost perfectly. However, the *ab initio* energies indicate that the linear complex is more tightly bound than we predict. Perhaps the nitrogen sp lone pair attracts the argon more strongly than the π-electrons do. The repulsive wall suggests that the SCF density is nearly spherically symmetric about each nitrogen atom, but the attractive well indicates significant anisotropy in the dispersion interaction. On the other hand, the Ar···F_2 complex provides an interesting contrast shown in Figure 9. The fluorine 2s lone pair appears to be significantly smaller than the 2p lone pairs leading to a strong anisotropy in the SCF repulsive wall that is nicely reproduced by the APF-D functional. The attractive wells for the Ar···F_2 complex are accurately described by our spherical dispersion model. Note that at all Ar···F distances the dispersion attraction of the two fluorine atoms to the argon in the C_{2v} complex is stronger than the attraction of the single close fluorine in the linear structure, but the SCF repulsion from the 2p lone pairs prevents the argon from getting as close in the C_{2v} structure as it does in the linear structure.

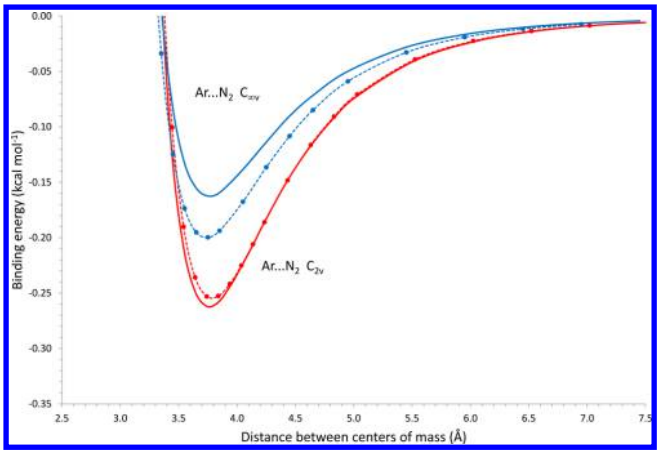

Figure 8. Dissociation energy curve of Ar···N_2 in both the linear ($C_{\infty v}$) and T−shaped (C_{2v}) conformation. Both APF-D/aug-cc-pVTZ (solid lines) and CCSD(T)/aug-cc-pVQZ (dashed lines with bullets) results are shown.

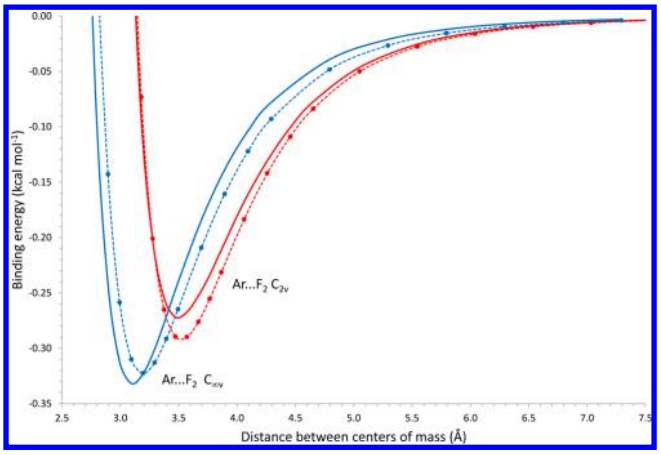

Figure 9. Dissociation energy curve of Ar···F_2 in both the linear ($C_{\infty v}$) and T-shaped (C_{2v}) conformation. Both APF-D/aug-cc-pVTZ (solid lines) and CCSD(T)/aug-cc-pVQZ (dashed lines with bullets) results are shown.

Atoms in molecules can deviate from spherical symmetry through either the SCF repulsion, as in F_2, or the dispersion attraction,as in N_2. The APF functional, and likely, most other functionals, correctly describes the anisotropy of the density at the SCF level. The anisotropy in the dispersive interactions such as the one exhibited by the nitrogen atoms in Ar···N_2 clearly represents a greater challenge.

The van der Waals complex of argon with P_2 shows similarities with the one involving N_2. In the case of Ar···P_2, the APF-D potential agrees with the CCSD(T) potential for the linear structure but overestimates the binding in the C_{2v} structure (see Figure S1 in the Supporting Information). This is consistent with recent studies of 3-body effects,[65−67] indicating a decrease in the polarizability of an atom that is adjacent to a strongly polarized atom. Inclusion of either 3-body interactions or anisotropy in 2-body interactions requires a far more complex theory and computationally expensive model than the simple APF-D functional. Note that, if we were to adjust the phosphorus parameters to reduce the attraction in the C_{2v} complex, we would then underestimate the binding in the linear complex. Likewise, if we were to adjust the nitrogen parameters to increase the attraction in the linear complex, we would then overestimate the binding in the C_{2v} complex. The difficulties we observe for N_2 and P_2 point out the inherent limitations that are likely to be present in any model with spherically symmetric van der Waals interactions between pairs of atoms.

We have emphasized some limitations of the APF-D functional for anisotropic atoms in molecules. It is important not to be overly enthusiastic about one's own models, but we should nevertheless emphasize their strengths. In particular, the dissociative portions of the potential energy curves in Figures 8 and 9 and Figure S1 (Supporting Information) are all described quite accurately by the APF-D functional, and the agreement with the CCSD(T)/CBS curve is remarkable. The difficulties arise in the region where the densities begin to overlap. As an example, in Figure 10, we show the complete dissociation curve of the Ar···O_2 complex. Both APF-D and B2PLYP-D3 give correct asymptotic R^{-6} interactions. However, at long-range B2PLYP-D3 appears to slightly double count the dispersion contribution from the second order energy correction and the empirical dispersion. Despite the fact that M05-2X gives reasonable geometries and binding energies, the latter decays

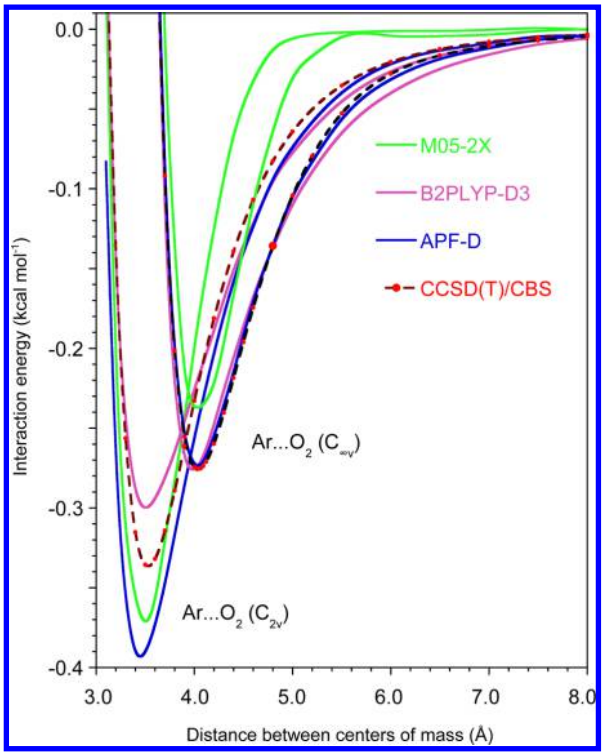

Figure 10. Dissociation energy curve of Ar···O_2 in both the linear ($C_{\infty v}$) and T-shaped (C_{2v}) conformation. All calculations were performed using the aug-cc-pVTZ basis set.

exponentially rather than as R^{-6}. As we already discussed in section 2.1, this is a major shortcoming common to all SCF-level density functionals that do not also include an empirical dispersion add-on.

4.3. Hydrocarbon Dimers. Hydrocarbons are generally nonpolar and thus offer polyatomic tests of dispersion models without the complication of strong electrostatic interactions. The calculated equilibrium geometries and binding energies for a sample of hydrocarbon dimers are reported in Tables 8 and 9. The first group includes dimers of methane (in two conformations), ethylene, and acetylene: these are smaller systems and most of them are included in the training set for the parametrization of our model. The second group includes the methane···benzene complex and the benzene dimer in three different conformers. For this group, the internal geometry of the monomers has been held fixed while the intermolecular distance has been optimized (see the Supporting Information for more details). The systems in this second group were not included in the training set of the APF-D functional and therefore serve as a test of the parameter adjustments collected in Table 3.

As expected, the APF-D functional shows remarkable accuracy for the systems in the first group, which is matched only by M05-2X both in terms of equilibrium geometry and binding energy. The PW86PBE-XDM(BR) method also provides very accurate binding energies. Both B97-D3 and B2PLYP-D3 are as accurate as CCSD(T) although the binding energies computed with B97-D3 are consistently overestimated. MP2 does not appear to be competitive with the other methods for these smaller hydrocarbon dimers.

The errors in the binding energies are larger across the board for the second group of dimers, all of which include the benzene molecule, with the exception of B97-D3. M05-2X,

dx.doi.org/10.1021/ct300778e | J. Chem. Theory Comput. 2012, 8, 4989−5007

Table 8. Equilibrium Geometries of Hydrocarbon Dimers[a]

	M05-2X	B97-D3	B2PLYP-D3	APF-D	MP2	CCSD(T)	CCSD(T)/CBS	ref
$HCH_3\cdots H_3CH$ D_{3d}	3.673	3.700	3.661	3.651	3.635	3.621	3.633	84
$H_3CH\cdots HCH_3$ D_{3d}	4.857	4.702	4.656	4.763	4.694	4.669	4.794	84
$(H_2C{=}CH_2)_2$ ×[b]	3.716	3.656	3.674	3.723	3.665	3.696	3.707	(T,Q)[c]
$(H{-}C{\equiv}C{-}H)_2$ ×	4.155	4.200	4.115	4.051	3.881	4.059	4.111	(T,Q)[c]
$(H{-}C{\equiv}C{-}H)_2$ ⊥	4.345	4.346	4.333	4.296	4.272	4.313	4.353	(T,Q)[c]
RMS error[d]	0.039	0.069	0.065	0.041	0.119	0.064		
$H_3CH\cdots C_6H_6$ ⊥ C_{3v}	3.783	3.734	3.707	3.712	3.715		3.76	85
$(C_6H_6)_2$ ⊥ C_{2v}	4.957	4.932	4.924	4.894	4.769	5.00	4.9	85
$(C_6H_6)_2$ ∥ D_{6h}	4.152	3.897	3.826	3.785	3.627	3.93	3.8	85
$(C_6H_6)_2$ ∥ C_{2h}	3.572	3.470	3.456	3.435	3.269	3.52	3.5	85
R[e]	1.903	1.785	1.679	1.642	1.553	1.71	1.7	85
RMS error[f]	0.187	0.062	0.036	0.045	0.158	0.083		

[a]The distances (in Å) between centers of mass of the monomers are reported. All calculations were performed using the aug-cc-pVTZ basis sets. CP corrections or CBS extrapolation were not performed unless explicitly stated. [b]The two planes containing the monomer intersect at right angle. [c]Extrapolated result using aug-cc-pVTZ and aug-cc-pVQZ basis sets. [d]Excluding $CH_4\cdots C_6H_6$ and $(C_6H_6)_2$; [e]Distance between the planes containing the two C_6H_6 molecules; [f]including only $CH_4\cdots C_6H_6$ and $(C_6H_6)_2$.

Table 9. Dissociation Energies of Hydrocarbon Dimers[a]

	M05-2X	B97-D3	B2PLYP-D3	PW86PBE XDM[b]	APF-D	APF-D CP	MP2	CCSD(T)	CCSD(T) CP	CCSD(T) CBS	ref
$HCH_3\cdots H_3CH$ D_{3d}	0.512	0.577	0.610	0.54	0.562	0.544	0.601	0.638	0.496	0.544	84
$H_3CH\cdots HCH_3$ D_{3d}	0.079	0.317	0.289		0.205	0.186	0.271	0.305	0.175	0.188	84
$(H_2C{=}CH_2)_2$ ×[c]	1.415	1.897	1.754	1.36	1.578	1.523	1.940	1.758	1.373	1.508	(T,Q)[d]
$(H{-}C{\equiv}C{-}H)_2$ ×	0.101	0.205	0.210		0.201	0.179	0.439	0.252	0.146	0.175	(T,Q)[d]
$(H{-}C{\equiv}C{-}H)_2$ ⊥	1.516	1.828	1.786	1.64	1.774	1.695	1.976	1.805	1.436	1.545	(T,Q)[d]
RMS error[e]	0.075	0.224	0.164	0.1	0.108	0.067	0.301	0.178	0.082		
$H_3CH\cdots C_6H_6$ ⊥ C_{3v}	1.244	1.585	1.940		1.677	1.584	2.438			1.44	85
$(C_6H_6)_2$ ⊥ C_{2v}	2.176	2.976	3.670	2.4	3.287	3.107	4.936	2.53	2.50	2.70	85
$(C_6H_6)_2$ ∥ D_{6h}	0.491	1.694	2.637	1.49	2.474	2.315	4.503	1.60	1.57	1.70	85
$(C_6H_6)_2$ ∥ C_{2h}	1.644	2.707	3.846	2.63	3.661	3.468	6.357	2.60	2.57	2.73	85
RMS error[f]	0.895	0.156	0.910	0.22	0.683	0.527	2.598	0.136	0.166		

[a]Energies are reported in kcal mol^{-1}. All calculations were performed using the aug-cc-pVTZ basis sets. CP corrections or CBS extrapolation were not performed unless explicitly stated. [b]Ref 28. [c]The two planes containing the monomer intersect at right angle. [d]Extrapolated result using aug-cc-pVTZ and aug-cc-pVQZ basis sets. [e]Excluding $CH_4\cdots C_6H_6$ and $(C_6H_6)_2$; [f]including only $CH_4\cdots C_6H_6$ and $(C_6H_6)_2$.

Table 10. Counterpoise Corrections to Equilibrium Distance and Binding Energy of the Perpendicular C_{2v} Conformation of the Benzene Dimer[a]

	basis set	M05-2X	B2PLYP-D3	APF-D	MP2	CCSD(T)
R	cc-pVDZ	0.100	0.084	0.052	0.206	
	aug-cc-pVDZ	0.142	0.098	0.043	0.217	
	aug-cc-pVTZ	0.013	0.034	0.012	0.140	
De	cc-pVDZ	0.51	0.93	0.67	1.49	3.36
	aug-cc-pVDZ	0.92	1.40	0.95	3.28	3.36
	aug-cc-pVTZ	0.24	0.49	0.18	1.56	1.49

[a]The distance (in Å) between the centers of mass of the monomers is optimized while the geometry of the monomers is held fixed (see the Supporting Information for details). The binding energies D_e are reported in kcal mol^{-1}.

B2PLYP-D3, and APF-D show a similar reduced accuracy while PW86PBE-XDM(BR) remains very accurate. While accurate geometries are provided by APF-D, B2PLYP-D3, and B97-D3, the same is not true in this case for M05-2X, which is as bad as MP2. It is important to note that the MP2 geometries are the worst of the lot, and this should serve as a warning against the rather common practice of adopting highly correlated single point energies at the MP2 optimized geometries as benchmarks of the binding energies of weakly bounded complexes.

The importance of CP corrections of BSSE on geometries and binding energies varies greatly with the basis set and the theoretical method. In Table 10, we explore the impact of BSSE for the perpendicular C_{2v} conformation of the benzene dimer. MP2 suffers the most in this respect, and this is likely due to a larger BSSE associated with the perturbative energy correction. Consistently, the effect of BSSE on the geometry and binding energy is smaller for B2PLYP-D3 than for MP2 since the former includes only a fraction of the perturbative energy correction. M05-2X and APF-D are both SCF-level methods and show similar BSSE errors in the binding energies, but M05-2X has larger BSSE errors in the equilibrium geometries. This is possibly due to the fact that the parameters in APF-D have been chosen considering whole dissociation curves rather than focusing only on the binding energy at the equilibrium distance.

The accuracy of the APF-D in reproducing long-range interactions is again notable. In Figure 11, we show the

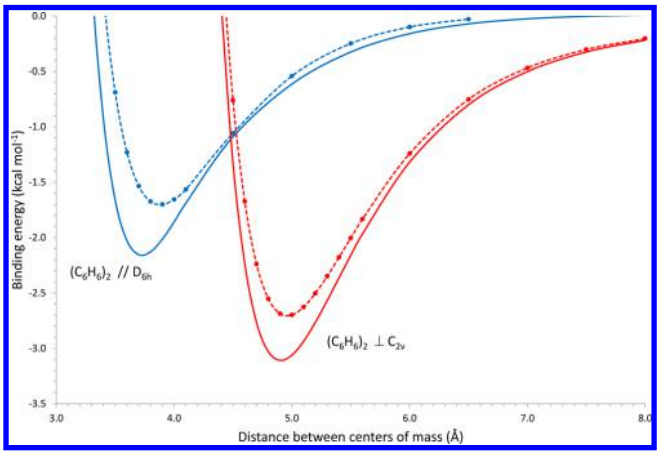

Figure 11. Dissociation energy curves of the benzene dimer in the stacked (D_{6h}) and T-shaped (C_{2v}) conformations. Both APF-D/aug-cc-pVTZ (solid lines) and CCSD(T)/aug-cc-pVTZ (dashed lines with bullets) results are shown.

potential energy curves for the stacked (D_{6h}) and "T-shaped" (C_{2v}) conformation of the benzene dimer. The excellent agreement between the long-range behavior of APF-D and CCSD(T) means that it would be very difficult to improve on our simple rules for estimating $C_{6,AB}$ and $R_{s,AB}$, from ionization potentials and polarizabilities, but it is possible that an adjustment to $R_{d,AB}$ could improve the accuracy of APF-D near the minimum. The value appropriate for the four hydrocarbon dimers in the training set may be too small for these species with multiple π-bonds. However, any adjustment of $R_{d,AB}$ to improve the agreement with CCSD(T) for the example in Figure 11 is likely to have a negative effect on the examples in Figure 7. At this time, we rather prefer to limit the number of adjustable parameters to the ones currently in the model, and not attempt any adjustment to improve the accuracy in the specific case of the benzene dimer. Similar considerations can be done for the potential energy curves of the methane···benzene and the C_{2v} conformation of the acetylene dimer (see Figures S2 and S3 in the Supporting Information).

4.4. Intramolecular Dispersion and Molecular Structure. Together with other kinds of interactions, dispersion forces can also play an important role in determining the relative energies of conformational and configurational isomers. For example, the *cis*-halopropenes are more stable than the corresponding *trans* isomers due in part to the dispersion attractions. In Table 11, we compare the relative stability of the *cis* and *trans* isomers of fluoro, chloro and bromo-propene as predicted by various methods, and we include 2-butene for comparison. We measure the accuracy with respect to the energy difference at the CCSD(T)/aug-cc-pVTZ level of theory (see ref 68 for details of the geometries used for the calculations in Table 11).

Hartree−Fock cannot correctly predict the relative stability of the *cis* and *trans* isomers of chloro and bromo-propene. On the other hand, the B3LYP functional (and probably most of the available DFT methods) does predict the correct relative stability but with a sizable RMS error. M05-2X, B97-D3, and MP2 are somewhat more accurate, while APF-D and the more costly B2PLYP-D3 provide the best accuracy, with a RMS error below 0.1 kcal mol^{-1}.

4.5. Hydrogen Bonds and Other Electrostatic Interactions. Dispersion forces can play an important role in determining the relative energies of conformational isomers, but hydrogen bonds and electrostatic interactions in general are likely to produce larger effects. The equilibrium distances and binding energies for a small selection of species with large electrostatic interactions are given in Tables 12 and 13. Following common practice for these species, we consistently employed the "S22 geometries" of the dimers[69] to avoid optimizing the geometries of all dimers with all methods, and to facilitate comparisons with previous studies.[70] Also following common practice for these species, all calculations in Tables 12 and 13 include CP corrections for BSSE. The distance between the monomers was varied along the noted direction and a polynomial fit was used to obtain the minimum energy geometries and energies.

All the methods in Table 12 provide a geometry that is accurate and adequate to be used for a higher level single point energy calculation. The only exception is B3LYP, which shows a large error in the interplanar distance of the stacked adenine−thymine complex, which is the system where dispersion forces are likely to be more important relative to electrostatic and hydrogen bonding interactions. Using the aug-cc-pVTZ basis set, the CCSD(T) equilibrium distances are consistently overestimated by about 0.03 Å, while those predicted by APF-D are consistently too short by about 0.03 Å.

To accurately predict the binding energies for the species in Table 13, the method must predict both accurate charge distributions and accurate dispersion interactions. The two configurations of the adenine−thymine complex provide a striking illustration of this point. If we separate the SCF energy from the empirical dispersion contribution in APF-D, the hydrogen bonded Watson−Crick complex is bound by the sum of ∼13 kcal mol^{-1} net SCF attraction, which represents the balance of electrostatic attraction and short-range Pauli exclusion repulsion, plus ∼4 kcal mol^{-1} of dispersion attraction. On the other hand, the π-bonded stacked complex is bound by

Table 11. Energy Difference (in kcal mol^{-1}) between the *cis* and *trans* Isomers of 1-Substitued Propenes[a]

	HF	B3LYP	M05-2X	B97-D3	B2PLYP-D3	APF-D	MP2	CCSD(T)
$CH_3CH{=}CHF$	−0.521	−0.567	−0.679	−0.526	−0.713	−0.726	−0.707	−0.653
$CH_3CH{=}CHCl$	0.101	−0.290	−0.546	−0.587	−0.630	−0.597	−0.763	−0.590
$CH_3CH{=}CHBr$	0.373	−0.164	−0.550	−0.547	−0.625	−0.712	−0.989	−0.784
$CH_3CH{=}CHCH_3$	1.640	1.240	1.236	1.085	1.035	1.022	1.039	1.054
RMS error[b]	0.738	0.359	0.150	0.135	0.088	0.054	0.137	

[a]See ref 69 and the Supporting Information for more details and for the specification of the molecular geometries. All calculations were performed using the aug-cc-pVTZ basis sets. [b]RMS error with respect to CCSD(T) results.

Table 12. Equilibrium Distance of Hydrogen Bond Complexes and Other Complexes with Strong Electrostatic Interactions[a]

	distance	B3LYP	M05-2X	B97-D3	B2PLYP-D3	APF-D	MP2	CCSD(T)	ref[b]
HO−H···OH_2 C_s	H···O	1.968	1.968	2.019	1.963	1.923	1.980	1.977	1.952
HO−H···NH_3 C_s	H···N	1.971	1.980	1.960	1.958	1.924	1.974	1.987	1.965
$(NH_3)_2$ C_{2h}	H···N	2.578	2.529	2.600	2.548	2.537	2.535	2.541	2.503
formic acid dimer C_{2h}	H···O	1.685	1.659	1.687	1.684	1.633	1.694	1.699	1.670
formamide dimer C_{2h}	H···O	1.868	1.869	1.871	1.855	1.805	1.864	1.869	1.841
adenine···thymine WC[c]	H···N	1.846	1.834	1.802	1.810	1.751	1.812	1.827[e]	1.819
adenine···thymine stack	/···/[d]	3.433	3.273	3.224	3.254	3.181	3.152	3.239[e]	3.186
RMS error		0.099	0.038	0.049	0.032	0.040	0.024	0.032	

[a]The equilibrium distances are reported in Å and are relative to a deformation of the complex in that specific direction while the geometry of the monomers is held fixed. All calculations were performed using the aug-cc-pVTZ basis sets and the results include CP corrections. [b]See ref 69 for the specification of the molecular geometries. [c]Watson−Crick conformation. [d]Distance between the planes of the two monomers. [e]Extrapolated geometry according to CCSD(T)/aug-cc-pVDZ + (MP2/aug-cc-pVTZ − MP2/aug-cc-pVDZ).

Table 13. Binding Energies of Hydrogen Bond Complexes and Other Complexes with Strong Electrostatic Interactions[a]

	B3LYP	M05-2X	B97-D3	B2PLYP-D3	PW86PBE XDM[b]	APF-D	MP2	CCSD(T)	CCSD(T) CBS[c]
HO−H···OH_2 C_s	4.47	5.14	4.61	5.13	5.23	5.22	4.69	4.73	5.02
HO−H···NH_3 C_s	6.12	6.61	6.54	6.86	7.12	7.22	6.35	6.26	6.61
$(NH_3)_2$ C_{2h}	2.18	3.13	2.99	3.15	3.24	3.02	2.99	2.99	3.17
formic acid dimer C_{2h}	17.33	19.62	18.08	19.06	19.13	21.22	17.55	17.76	18.80
formamide dimer C_{2h}	13.98	16.00	15.16	16.19	16.09	17.07	15.03	15.29	16.12
adenine···thymine WC[d]	12.81	14.90	15.91	16.70	16.68	17.77	15.80	15.94	16.74
adenine···thymine stack	−1.40	9.18	10.45	12.00	10.07	13.75	14.26	11.13	11.66
RMS error	5.27	1.21	0.74	0.19	0.65	1.34	1.23	0.47	
RMS % relative error	45.49	9.26	6.35	2.08	6.22	9.88	10.07	5.27	

[a]The binding energies are reported in kcal mol^{-1}. All calculations were performed using the aug-cc-pVTZ basis sets and the results include CP corrections. [b]Ref 28. [c]Ref 70. [d]Watson−Crick conformation.

~4 kcal mol^{-1} SCF attraction plus ~13 kcal mol^{-1} of dispersion.

All models in Table 13 with dispersion interactions give a reasonable description of the two adenine−thymine structures. Indeed, the large errors shown by the B3LYP results, where there is no attempt to include dispersion, constitute a qualitative measure of the importance of dispersion in the stacked dimer. The interaction energies computed by MP2 slightly underestimate the strength of hydrogen bonds, but appear to overestimate the dispersion interaction in the adenine−thymine stacked complex. The corrections provided by higher order correlation methods like CCSD(T) are very small for the strongly hydrogen bonded species, but they exceed 3 kcal mol^{-1} for the adenine−thymine stacked configuration. For all the species in Table 13, CCSD(T) with a finite basis set and inclusion of CP corrections provides a slightly underestimated binding energy. The CP correction to the APF-D/aug-cc-pVTZ binding energies is generally small and amounts to less than 0.4 kcal mol^{-1} for all species in Table 13.

The equilibrium distances of the hydrogen bonded species are consistently underestimated by APF-D because the model slightly overestimates the binding near the minimum. Nevertheless, APF-D accurately follows the long-range portion of the CCSD(T) potential energy curve. The most strongly bound species and thus the one with the shortest hydrogen bonds is the formic acid dimer, which is over bound by more than 2 kcal mol^{-1}, but the dissociative portion of the potential energy curve is virtually identical to the one of the CCSD(T) curve (see Figure S4 in the Supporting Information). In Figure 12, we show that the APF-D potential energy curve for the Watson−Crick structure of the adenine−thymine complex shows similar

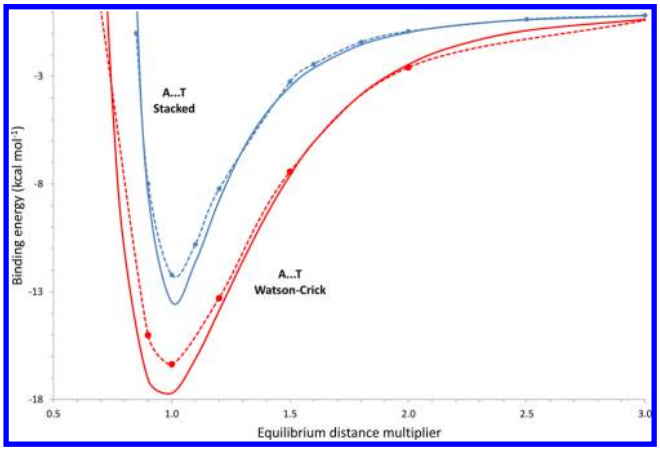

Figure 12. Dissociation energy curves of the adenine−thymine complex in the stacked and in the Watson−Crick conformations. Both APF-D/aug-cc-pVTZ (solid lines) and CCSD(T)/aug-cc-pVTZ (dashed lines with bullets) results are shown.

behavior. The stacked adenine−thymine complex is dominated by the rapid R^{-6} decay of the dispersion interaction, rather than the more gradual R^{-3} decay of the electrostatic interactions which dominate the Watson−Crick complex. This implies that both the description of the electrostatic potential at large distances provided by APF and the $C_{6,AB}$ coefficient included in the empirical dispersion model are correct. The over binding around the minimum energy geometry must be the result of deficiencies in $R_{s,AB}$ and/or $R_{d,AB}$. In addition, it is worth noting that strongly bound species such as those in Table 13 can induce significant geometry changes in the monomers. In the "S22 geometries" the monomer structure has been optimized to

Table 14. Comparison of RMS Errors (in Å) for Bond Lengths of 101 Diatomic Molecules Collected in Three Separate Sets According to the Heaviest Element Involved[a]

	B3LYP	M05-2X	M06-2X	APF-D	HF	MP2[b]	CCSD(T)[b]
H−F (22)	0.011	0.015	0.013	0.012	0.029	0.013	0.010
Na−Cl (25)	0.026	0.017	0.015	0.018	0.030	0.014	0.015
K−Br (54)	0.029	0.042	0.049	0.026	0.080	0.041	0.021

[a]See the Supporting Information for a list of molecules and reference values of the bond lengths. [b]Includes Na(2s,2p), K(3s,3p), Ca(3s,3p), Sc(3s,3p), Ga(3d), and Ge(3d) electron correlation.

Table 15. Errors in Total Atomization Energies at 298 K (TAE), Ionization Potentials (IP), Electron Affinities (EA), and Proton Affinities (PA) for Selected Molecules in the G2/97 Test Set[a,b], Together with Six Bond Dissociation Energies (BDE) of Spin Contaminated Species in the W1 Test Set[b,c]

		B3LYP	M05-2X	M06	M06-2X	APF-D	W1-BD
	MAD	2.64	2.59	2.53	1.79	2.85	0.61
TAE (81)	RMS	3.49	3.59	3.33	2.43	3.60	0.77
	MAX	−12.07	−11.12	8.72	−10.12	−9.84	1.97
	MAD	3.68	2.67	3.43	2.21	3.94	0.35
IP (76)	RMS	4.73	3.84	4.13	3.11	4.71	0.46
	MAX	−13.47	15.13	−11.52	11.36	−14.19	−1.42
	MAD	2.71	2.39	2.19	2.08	2.89	0.43
EA (55)	RMS	3.72	3.40	2.61	2.85	3.33	0.55
	MAX	10.80	11.03	5.53	10.27	−7.04	−1.81
	MAD	1.01	0.85	1.44	1.37	1.40	0.42
PA (8)	RMS	1.16	1.05	1.74	1.31	1.50	0.49
	MAX	2.07	1.96	3.49	−2.11	2.19	−0.83
	MAD	2.08	5.57	3.59	5.91	2.07	0.55
BDE (6)	RMS	2.31	6.45	4.24	7.51	2.36	0.74
	MAX	−3.92	−10.67	−6.69	13.12	−3.89	1.10
	MAD	2.93	2.59	2.74	2.11	3.15	0.47
total (226)	RMS	3.93	3.68	3.46	3.00	3.88	0.62
	MAX	−13.47	15.13	−11.52	13.12	−14.19	1.97

[a]Ref 86. [b]Ref 72. [c]Mean absolute (MAD), root mean square (RMS), and maximum absolute (MAX) errors are reported in kcal mol^{-1}. All DFT calculations were performed using the aug-cc-pVQZ basis sets. W1-DB[b] results are included for comparison.

Table 16. Equilibrium Bond Lengths (in Å) of Alkali and Alkaline Earth Dimers[a]

		M05-2X	B97-D3	B2PLYP-D3	APF	APF-D	MP2	CCSD(T)	CCSD(T)[b]	exp.	ref
alkali	Li−Li	2.707	2.769	2.713	2.728	2.726	2.750	2.700		2.6729	87
	Na−Na	2.984	3.219	3.096	3.094	3.083	3.177	3.098		3.0786	88
	K−K	3.799	4.103	4.006	3.950	3.859	4.039	3.966		3.924	89
	Cu−Cu	2.335	2.272	2.261	2.268	2.145	2.236	2.258		2.2197	90
RMS error		0.099	0.126	0.051	0.040	0.056	0.085	0.033			
alkaline earth	Be···Be	2.646	2.582	2.565	2.497	2.399	2.78	2.533	2.502	2.438	91
	Mg···Mg	3.857	3.769	3.946	3.595	3.627	4.138	4.056	3.934	3.891	92
	Ca···Ca	4.411	4.424	4.573	4.203	4.204	4.564	4.431	4.347	4.277	93
	Zn···Zn	3.847	3.516	3.664	3.334	3.334	3.715	4.009	3.978	3.847(b)	93
RMS error		0.125	0.204	0.187	0.300	0.291	0.264	0.147	0.084		

[a]All calculations were performed using the aug-cc-pVTZ basis set where available and a basis set of similar quality otherwise (see Supporting Information for details). [b]CCSD(T)/aug-cc-pCVQZ.

minimize the energy of the dimer.[69,70] For example, in the case of the formic acid dimer, the APF-D/aug-cc-pVTZ binding energy is smaller by about 3 kcal mol^{-1} if we form the dimer using monomers at their fixed optimized geometry. Therefore, a better assessment of the binding energy of the kind of complexes discussed in this section should likely involve full geometry optimization along the whole dissociation curve.

4.6. Covalent and Ionic Molecules. A density functional augmented with an empirical dispersion add-on is useful only if it also provides reliable geometries and energies for molecules involving mainly covalent and ionic bonds. We ensured this in the case of the APF functional by using a linear combination of the B3PW91 and PBE1PBE functionals, which had been extensively tested and thoroughly calibrated with standard sets of thermochemical data. Nevertheless, it is important to verify that we have not introduced significant errors in the geometry or thermochemistry of covalent and ionic species. We have therefore examined the accuracy of APF-D in predicting the geometries of over 100 diatomic molecules with known equilibrium geometries and the thermochemistry of more than 200 examples from the W1 test set.[71]

Table 17. Dissociation Energies (in kcal mol^{-1}) of Alkali and Alkaline Earth Dimers[a]

		M05-2X	B97-D3	B2PLYP-D3	APF	APF-D	MP2	CCSD(T)	CCSD(T)[b]	exp.	ref
alkali	Li−Li	27.53	28.11	20.99	19.06	19.09	17.30	23.81		24.351	87
	Na−Na	26.36	32.80	16.10	14.83	14.96	11.56	16.53		17.218	88
	K−K	23.77	31.97	10.06	10.57	11.34	7.21	11.55		12.7251	89
	Cu−Cu	48.48	53.32	43.15	41.02	48.37	43.17	42.52		47.1	90
RMS error		7.38	12.90	2.97	4.34	3.01	5.65	2.40			
alkaline earth	Be···Be	2.53	6.64	2.66	6.36	9.45	1.05	1.29	1.64	2.672	91
	Mg···Mg	1.20	5.54	2.55	2.30	2.39	0.92	0.91	1.29	1.21	92
	Ca···Ca	2.89	9.46	4.98	4.62	4.71	2.08	2.79	2.56	3.151	93
	Zn···Zn	0.77	3.80	1.94	0.95	0.95	0.99	0.42	0.51	0.646[(d)]	63
RMS error		0.16	4.59	1.31	2.06	3.53	1.00	0.74	0.60		

[a]All calculations were performed using the aug-cc-pVTZ basis set where available and a basis set of similar quality otherwise (see the Supporting Information for details). [b]CCSD(T)/aug-cc-pCVQZ.

In Table 14, we report the RMS errors for the prediction of the bond lengths of 101 diatomic molecules (see the Supporting Information for a list of the molecules and the reference bond lengths). We divided the results into three sets according to the heaviest element in the diatomic. The overall accuracy of APF-D/aug-cc-pVTZ is slightly inferior that of CCSD(T)/aug-cc-pVTZ, but it certainly remains competitive with both MP2 and other widely used density functionals.

The results in Table 15 illustrate the accuracy of various methods on 226 examples from the W1 test set. We considered atomization energies at 298 K, ionization potentials, electron affinities, proton affinities, and bond dissociation energies. We include the results of the W1-BD[88] method, which give an idea of the kind of accuracy it is possible to achieve, although at a computational cost orders of magnitude greater than that of a standard DFT method. Overall, there is little difference in the performance of the five functionals in Table 15. This confirms that APF-D is at least as accurate as other widely used functionals in predicting standard thermochemical quantities.

4.7. Alkali and Alkaline Earth Dimers. The prediction of equilibrium geometry and dissociation energy of species such as alkali and alkaline earth dimers presents specific difficulties that justify their treatment as a separate group. The results collected in Tables 16 and 17 illustrate how challenging these species actually are.

The MP2 and CCSD(T) calculations on the alkali metal dimers require the inclusion of core electron correlation (2s and 2p for Na, 3s and 3p for K, and 3d for Cu) to avoid errors in excess of 0.1 Å in the equilibrium distances. To achieve similar accuracy on the alkaline earth dimers, we need to expand the basis set used for the CCSD(T) calculations to aug-cc-pCVQZ. The alkali metal dimers are joined by weak covalent bonds, whereas the alkaline earth dimers are generally considered van der Waals complexes. Nevertheless, dispersion forces from core electrons play an important role in both.

For the alkali metal dimers, the accuracy of APF-D is comparable to that of B2PLYP-D3 and CCSD(T), both for the equilibrium distances and the binding energies. The situation is different for the alkaline earth dimer, where B2PLYP-D3 becomes superior with respect to APF-D. The APF-D bond lengths of Na_2 and K_2 are too long if we omit the dispersion interactions, but the Cu_2 bond length becomes too short when we include them. None of the methods included in Table 16 maintain errors below 0.1 Å for all eight dimers. The B2PLYP-D3, APF-D, and CCSD(T) methods give useful geometries for the alkali metal dimers, but none of the calculations in Table 16 give results for the alkaline earth dimers of the same accuracy seen for the other systems considered.

All the binding energies for the alkali metal dimers are underestimated, with the sole exception of the M05-2X values, which have some of the largest errors. However, M05-2X is the only method that gives useful binding energies for the alkaline earth dimers. It is rather curious that the M05-2X binding energies for Be_2 and Ca_2 are quite reasonable, even though the bond lengths are 0.2 Å too long. The APF potential for the alkaline earth dimers includes a spurious attraction that consistently exaggerates binding, and produces bond lengths for Mg_2 and Zn_2 that are much too short.

Overall, the CCSD(T)/CBS limit should be adequate for both the geometry and the binding energy of all these species, but none of the other methods included in Tables 16 and 17 is up to the task.

5. CONCLUSIONS

The APF functional has been designed to provide cancellation between the spurious exponentially decaying long-range attractions and repulsions generally present in other functionals. The addition of an empirical term based on a spherical atom model (SAM) for dispersion interactions, completes the definition of the APF-D model.

The accuracy of APF-D has been assessed using a diverse set of systems including noble gas dimers, argon complexes with nonpolar molecules, and dimers of small hydrocarbons. Overall the accuracy of APF-D has been found to be comparable to that of B2PLYP-D3 and CCSD(T), when the aug-cc-pVTZ basis is used. However, both B2PLYP-D3 and CCSD(T) involve a much larger computational cost than APF-D.

The binding energies are typically overestimated up to 10% by APF-D at the shorter distances found in dimers of larger hydrocarbons such as benzene and in complexes involving hydrogen bonds. Nevertheless, the inspection of the actual dissociation energy profiles show that starting at about 1.2 × the equilibrium distance, the APF-D and CCSD(T) curves are effectively superimposed and show the correct R^{-6} decay, all the way to the dissociation limit for all the species considered in this work.

The geometry and thermochemistry provided by APF-D for a large set of covalent and ionic species are comparable in accuracy to other widely used density functionals.

Future work will likely involve a reexamination of the training set and the combination rules to obtain the atomic radii, $R_{s,AB}$ and $R_{d,AB}$, from the ionization potentials in an effort to reduce the errors in hydrogen bonded complexes and other

complexes of aromatic species, which involve interaction among many π-electrons. Our conclusion is that APF-D achieves an accuracy comparable to that of B2PLYP-D3, without resorting to large data sets for interpolating the C_6 parameters, showing a more rapid convergence with basis set and requiring a smaller computation cost.

■ ASSOCIATED CONTENT

Supporting Information

Detailed specification of the basis set used for the elements He, Ne, Ar, Kr, Xe, K, Ca, Cu, and Zn. Geometries of the nonpolar dimers in Tables 6 and 7, the hydrocarbon dimers including benzene in Tables 8 and 9, the *cis* and *trans* isomers in Table 11 and the 101 diatomic molecules used to compile the results in Table 14. Dissociation energy curve of Ar···P_2 in both the linear ($C_{\infty v}$) and T-shaped (C_{2v}) conformation, acetylene dimer in the T-shaped (C_{2v}) conformation, methane−benzene complex in the C_{3v} conformation, and formic acid dimer. This material is available free of charge via the Internet at http://pubs.acs.org/.

■ AUTHOR INFORMATION

Corresponding Author

*E-mail: gpetersson@wesleyan.edu.

Notes

The authors declare no competing financial interest.

■ ACKNOWLEDGMENTS

The authors acknowledge support from Gaussian, Inc., and Wesleyan University for computational facilities supported by National Science Foundation Grant No. CNS-0959856.

■ REFERENCES

(1) (a) Pople, J. In *Energy, Structure, and Reactivity*; Smith, D., McRae, W., Eds.; Wiley: New York, 1973; p 51. (b) Pople, J.; Binkley, J.; Seeger, R. *Int. J. Quantum Chem., Quantum Chem. Symp.* **1976**, *10*, 1−19. (c) Krishnan, R.; Pople, J. A. *Int. J. Quantum Chem.* **1978**, *14*, 91−100.

(2) For reviews on accurate computational thermochemistry, see, for example: (a) Helgaker, T.; Klopper, W.; Halkier, A.; Bak, K. L.; Jørgensen, P.; Olsen, J. In *Quantum-Mechanical Prediction of Thermochemical Data*; Cioslowski., J., Ed.; Kluwer Academic: Dordrecht, 2001; pp 1−30; (b) Martin, J. M. L.; Parthiban, S. In *Quantum-Mechanical Prediction of Thermochemical Data*; Cioslowski., J., Ed.; Kluwer Academic: Dordrecht, 2001; pp 31−65; (c) Raghavachari, K.; Curtiss, L. A. In *Quantum-Mechanical Prediction of Thermochemical Data*; Cioslowski., J., Ed.; Kluwer Academic: Dordrecht, 2001; pp 67−98; (d) Petersson, G. A.; In *Quantum-Mechanical Prediction of Thermochemical Data*; Cioslowski., J., Ed.; Kluwer Academic: Dordrecht, 2001; pp 99−130; (e) Henry, D. J.; Radom, L.; In *Quantum-Mechanical Prediction of Thermochemical Data*; Cioslowski., J., Ed.; Kluwer Academic: Dordrecht, 2001; pp 161−197.

(3) Montgomery, J. A.; Frisch, M. J.; Ochterski, J. W.; Petersson, G. A. *J. Chem. Phys.* **1999**, *110*, 2822−2827.

(4) Parthiban, S.; Martin, J. M. L. *J. Chem. Phys.* **2001**, *114*, 6014−6029.

(5) Andersson, Y.; Langreth, D. C.; Lundqvist, B. I. *Phys. Rev. Lett.* **1996**, *76*, 102−105.

(6) Savin, A. In *Recent Developments and Applications Of Modern Density Functional Theory*; Seminario, J. M., Ed.; Elsevier: Amsterdam, 1996; pp 327−358.

(7) Leininger, T.; Stoll, H.; Werner, H. J.; Savin, A. *Chem. Phys. Lett.* **1997**, *275*, 151−160.

(8) Iikura, H.; Tsuneda, T.; Yanai, T.; Hirao, K. *J. Chem. Phys.* **2001**, *115*, 3540−3544.

(9) Kamiya, M.; Tsuneda, T.; Hirao, K. *J. Chem. Phys.* **2002**, *117*, 6010−6015.

(10) Dion, M.; Rydberg, H.; Schroder, E.; Langreth, D. C.; Lundqvist, B. I. *Phys. Rev. Lett.* **2004**, *92*, 246401.

(11) (a) Becke, A. D.; Johnson, E. R. *J. Chem. Phys.* **2005**, *123*, 154101. (b) Becke, A. D.; Johnson, E. R. *J. Chem. Phys.* **2005**, *122*, 154104. (c) Becke, A. D.; Johnson, E. R. *J. Chem. Phys.* **2006**, *124*, 14104. (d) Becke, A. D.; Johnson, E. R. *J. Chem. Phys.* **2007**, *127*, 154108. (e) Johnson, E. R.; Becke, A. D. *J. Chem. Phys.* **2005**, *123*, 24101. (f) Johnson, E. R.; Becke, A. D. *J. Chem. Phys.* **2006**, *124*, 174104.

(12) Sato, T.; Tsuneda, T.; Hirao, K. *J. Chem. Phys.* **2007**, *126*, 234114.

(13) Thonhauser, T.; Cooper, V. R.; Li, S.; Puzder, A.; Hyldgaard, P.; Langreth, D. C. *Phys. Rev. B* **2007**, *76*, 125112.

(14) Johnson, E. R.; Mackie, I. D.; DiLabio, G. A. *J. Phys. Org. Chem.* **2009**, *22*, 1127−1135.

(15) Wu, X.; Vargas, M. C.; Nayak, S.; Lotrich, V.; Scoles, G. *J. Chem. Phys.* **2001**, *115*, 8748−8757.

(16) Wu, Q.; Yang, W. T. *J. Chem. Phys.* **2002**, *116*, 515−524.

(17) Grimme, S. *J. Comput. Chem.* **2004**, *25*, 1463−1473.

(18) Grimme, S. *J. Comput. Chem.* **2006**, *27*, 1787−99.

(19) Ortmann, F.; Bechstedt, F.; Schmidt, W. G. *Phys. Rev. B* **2006**, *73*, 205101.

(20) Jurecka, P.; Cerny, J.; Hobza, P.; Salahub, D. R. *J. Comput. Chem.* **2007**, *28*, 555−569.

(21) Chai, J. D.; Head-Gordon, M. *Phys. Chem. Chem. Phys.* **2008**, *10*, 6615−6620.

(22) von Lilienfeld, O. A.; Tavernelli, I.; Rothlisberger, U.; Sebastiani, D. *Phys. Rev. Lett.* **2004**, *93*, 153004.

(23) Lin, I. C.; Coutinho-Neto, M. D.; Felsenheimer, C.; von Lilienfeld, O. A.; Tavernelli, I.; Rothlisberger, U. *Phys. Rev. B* **2007**, *75*, 205131.

(24) Sun, Y. Y.; Kim, Y. H.; Lee, K.; Zhang, S. B. *J. Chem. Phys.* **2008**, *129*, 154102.

(25) DiLabio, G. A. *Chem. Phys. Lett.* **2008**, *455*, 348−353.

(26) Grimme, S.; Antony, J.; Ehrlich, S.; Krieg, H. *J. Chem. Phys.* **2010**, *132*, 154104.

(27) Kristyan, S.; Pulay, P. *Chem. Phys. Lett.* **1994**, *229*, 175−180.

(28) Kannemann, F. O.; Becke, A. D. *J. Chem. Theory Comput.* **2010**, *6*, 1081−1088.

(29) (a) Becke, A. D. *J. Chem. Phys.* **1993**, *98*, 5648−5652. (b) Stephens, P. J.; Devlin, F. J.; Chabalowski, C. F.; Frisch, M. J. *J. Phys. Chem.* **1994**, *98*, 11623−11627.

(30) Eisenschitz, R.; London, F. *Z. Phys.* **1930**, *60*, 491−527.

(31) Hirschfelder, J. O.; Curtiss, C.; Bird, R. B. *Molecular Theory of Gases and Liquids*; Wiley: New York, 1964.

(32) Pernal, K.; Podeszwa, R.; Patkowski, K.; Szalewicz, K. *Phys. Rev. Lett.* **2009**, *103*, 263201.

(33) Podeszwa, R.; Szalewicz, K. *J. Chem. Phys.* **2012**, *136*, 161102.

(34) (a) Steinmann, S. N.; Corminboeuf, C. *J. Chem. Theory Comput.* **2010**, *6*, 1990−2001. (b) Steinmann, S. N.; Corminboeuf, C. *J. Chem. Theory Comput.* **2011**, *7*, 3567−3577. (c) Steinmann, S. N.; Corminboeuf, C. *J. Chem. Phys.* **2011**, *134*, 044117.

(35) Boys, S. F.; Bernardi, F. *Mol. Phys.* **1970**, *19*, 553.

(36) Bartlett, R. J.; Purvis, G. D. *Int. J. Quantum Chem.* **1978**, *14*, 561−581.

(37) Purvis, G. D.; Bartlett, R. J. *J. Chem. Phys.* **1982**, *76*, 1910−1918.

(38) Pople, J. A.; Headgordon, M.; Raghavachari, K. *J. Chem. Phys.* **1987**, *87*, 5968−5975.

(39) Raghavachari, K.; Trucks, G. W.; Pople, J. A.; Headgordon, M. *Chem. Phys. Lett.* **1989**, *157*, 479−483.

(40) Murray, E. D.; Lee, K.; Langreth, D. C. *J. Chem. Theory Comput.* **2009**, *5*, 2754−2762.

(41) (a) Perdew, J. P.; Chevary, J. A.; Vosko, S. H.; Jackson, K. A.; Pederson, M. R.; Singh, D. J.; Fiolhais, C. *Phys. Rev. B* **1992**, *46*, 6671−6687. (b) Perdew, J. P.; Chevary, J. A.; Vosko, S. H.; Jackson, K. A.; Pederson, M. R.; Singh, D. J.; Fiolhais, C. *Phys. Rev. B* **1993**, *48*, 4978−4978.

(42) (a) Adamo, C.; Barone, V. *J. Chem. Phys.* **1999**, *110*, 6158−6170. (b) Perdew, J. P.; Burke, K.; Ernzerhof, M. *Phys. Rev. Lett.* **1996**, *77*, 3865−3868. (c) Perdew, J. P.; Burke, K.; Ernzerhof, M. *Phys. Rev. Lett.* **1997**, *78*, 1396−1396.
(43) Zhao, Y.; Schultz, N. E.; Truhlar, D. G. *J. Chem. Theory Comput.* **2006**, *2*, 364−382.
(44) Tao, J.; Perdew, J. P.; Staroverov, V. N.; Scuseria, G. E. *Phys. Rev. Lett.* **2003**, *91*, 146401.
(45) Schwabe, T.; Grimme, S. *Phys. Chem. Chem. Phys.* **2006**, *8*, 4398−4401.
(46) Austin, A. Ph.D. thesis, Wesleyan University, 2009.
(47) Brooks, F. C. *Phys. Rev.* **1952**, *86*, 92−97.
(48) Koide, A. *J. Phys. B: At., Mol. Opt. Phys.* **1976**, *9*, 3173−3183.
(49) Krauss, M.; Neumann, D. B. *J. Chem. Phys.* **1979**, *71*, 107−112.
(50) Musher, J. I.; Amos, A. T. *Phys. Rev.* **1967**, *164*, 31.
(51) Tang, K. T.; Toennies, J. P. *J. Chem. Phys.* **1984**, *80*, 3726−3741.
(52) Ahlrichs, R.; Penco, R.; Scoles, G. *Chem. Phys.* **1977**, *19*, 119−130.
(53) Elstner, M.; Hobza, P.; Frauenheim, T.; Suhai, S.; Kaxiras, E. *J. Chem. Phys.* **2001**, *114*, 5149−5155.
(54) Zimmerli, U.; Parrinello, M.; Koumoutsakos, P. *J. Chem. Phys.* **2004**, *120*, 2693−2699.
(55) Grimme, S.; Ehrlich, S.; Goerigk, L. *J. Comput. Chem.* **2011**, *32*, 1456−1465.
(56) Cybulski, S. M.; Toczylowski, R. R. *J. Chem. Phys.* **1999**, *111*, 10520−10528.
(57) Roothaan, C. C. J. *J. Chem. Phys.* **1951**, *19*, 1445−1458.
(58) Stratmann, R. E.; Scuseria, G. E.; Frisch, M. J. *Chem. Phys. Lett.* **1996**, *257*, 213−223.
(59) London, F. *Trans. Faraday Soc.* **1937**, *33*, 8−26.
(60) Katriel, J.; Davidson, E. R. *Proc. Natl. Acad. Sci. U.S.A.* **1980**, *77*, 4403−4406.
(61) Becke, A. D. *J. Chem. Phys.* **1997**, *107*, 8554−8560.
(62) (a) DeYonker, N. J.; Peterson, K. A.; Wilson, A. K. *J. Phys. Chem. A* **2007**, *111*, 11383−11393. (b) Balabanov, N. B.; Peterson, K. A. *J. Chem. Phys.* **2005**, *123*, 64107. (c) Prascher, B. P.; Woon, D. E.; Peterson, K. A.; Dunning, T. H.; Wilson, A. K. *Theor. Chem. Acc.* **2011**, *128*, 69−82. (d) Koput, J.; Peterson, K. A. *J. Phys. Chem. A* **2002**, *106*, 9595−9599.
(63) Peterson, K. A.; Puzzarini, C. *Theor. Chem. Acc.* **2005**, *114*, 283−296.
(64) Zhao, Y.; Truhlar, D. G. *J. Phys. Chem. A* **2006**, *110*, 13126−13130.
(65) Tkatchenko, A.; DiStasio, J.; Robert, A.; Car, R.; Scheffler, M. *Phys. Rev. Lett.* **2012**, *108*, 236402.
(66) Tkatchenko, A.; Scheffler, M. *Phys. Rev. Lett.* **2009**, *102*, 073005.
(67) Cole, M. W.; Velegol, D.; Kim, H. Y.; Lucas, A. A. *Mol. Simul.* **2009**, *35*, 849−866.
(68) Wiberg, K. B.; Wang, Y. G.; Petersson, G. A.; Bailey, W. F. *J. Chem. Theory Comput.* **2009**, *5*, 1033−1037.
(69) Jurecka, P.; Sponer, J.; Cerny, J.; Hobza, P. *Phys. Chem. Chem. Phys.* **2006**, *8*, 1985−93.
(70) Takatani, T.; Hohenstein, E. G.; Malagoli, M.; Marshall, M. S.; Sherrill, C. D. *J. Chem. Phys.* **2010**, *132*, 144104.
(71) Parthiban, S.; Martin, J. M. L. *J. Chem. Phys.* **2001**, *114*, 6014−6029.
(72) Barnes, E. C.; Petersson, G. A.; Montgomery, J. A.; Frisch, M. J.; Martin, J. M. L. *J. Chem. Theory Comput.* **2009**, *5*, 2687−2693.
(73) Ogilvie, J. F.; Wang, F. Y. H. *J. Mol. Struct.* **1992**, *273*, 277−290.
(74) Ogilvie, J. F.; Wang, F. Y. H. *J. Mol. Struct.* **1993**, *291*, 313−322.
(75) Kannemann, F. O.; Becke, A. D. *J. Chem. Theory Comput.* **2009**, *5*, 719−727.
(76) Bissonnette, C.; Chuaqui, C. E.; Crowell, K. G.; LeRoy, R. J.; Wheatley, R. J.; Meath, W. J. *J. Chem. Phys.* **1996**, *105*, 2639−2653.
(77) Heijman, T. G. A.; Korona, T.; Moszynski, R.; Wormer, P. E. S.; vanderAvoird, A. *J. Chem. Phys.* **1997**, *107*, 902−913.
(78) Fernandez, B.; Koch, H.; Makarewicz, J. *J. Chem. Phys.* **1999**, *110*, 8525−8532.
(79) Cybulski, S. M.; Kendall, R. A.; Chalasinski, G.; Severson, M. W.; Szczesniak, M. M. *J. Chem. Phys.* **1997**, *106*, 7731−7737.
(80) Chan, K. W.; Power, T. D.; Jai-nhuknan, J.; Cybulski, S. M. *J. Chem. Phys.* **1999**, *110*, 860−869.
(81) Doyle, R. J.; Hirst, D. M.; Hutson, J. M. *J. Chem. Phys.* **2006**, *125*, 184312.
(82) Cybulski, S. M.; Holt, J. S. *J. Chem. Phys.* **1999**, *110*, 7745−7755.
(83) Prosmiti, R.; Cunha, C.; Villarreal, P.; Delgado-Barrio, G. *J. Chem. Phys.* **2002**, *116*, 9249.
(84) Hellmann, R.; Bich, E.; Vogel, E. *J. Chem. Phys.* **2008**, 128.
(85) Sherrill, C. D.; Takatani, T.; Hohenstein, E. G. *J. Phys. Chem. A* **2009**, *113*, 10146−59.
(86) Curtiss, L. A.; Redfern, P. C.; Raghavachari, K.; Pople, J. A. *J. Chem. Phys.* **1998**, *109*, 42−55.
(87) Le Roy, R. J.; Dattani, N. S.; Coxon, J. A.; Ross, A. J.; Crozet, P.; Linton, C. *J. Chem. Phys.* **2009**, *131*, 204309.
(88) Matsunaga, N.; Zavitsas, A. A. *J. Chem. Phys.* **2004**, *120*, 5624−30.
(89) Zavitsas, A. A. *J. Chem. Phys.* **2006**, *124*, 144318.
(90) Morse, M. D. *Chem. Rev.* **1986**, *86*, 1049−1109.
(91) Patkowski, K.; Spirko, V.; Szalewicz, K. *Science* **2009**, *326*, 1382−4.
(92) Li, P.; Xie, W.; Tang, K. T. *J. Chem. Phys.* **2010**, *133*, 084308.
(93) Allard, O.; Pashov, A.; Knockel, H.; Tiemann, E. *Phys. Rev. A* **2002**, *66*.